Science of the Total Environment 827 (2022) 154149

Contents lists available at ScienceDirect

Science of the Total Environment

journal homepage: www.elsevier.com/locate/scitotenv

Nitrogen-enriched discharges from a highly managed watershed intensify red tide (*Karenia brevis*) blooms in southwest Florida

Miles Medina [a,*], David Kaplan [a], Eric C. Milbrandt [b], Dave Tomasko [c], Ray Huffaker [d], Christine Angelini [a]

[a] Center for Coastal Solutions, Engineering School for Sustainable Infrastructure and the Environment, University of Florida, Gainesville, FL, United States
[b] Marine Laboratory, Sanibel-Captiva Conservation Foundation, Sanibel, FL, United States
[c] Sarasota Bay Estuary Program, Sarasota, FL, United States
[d] Department of Agricultural and Biological Engineering, University of Florida, Gainesville, FL, United States

HIGHLIGHTS

- Anthropogenic forcing is a key component of coastal *K. brevis* bloom dynamics.
- Nonlinear time series methods reveal state-dependent causal connections.
- Caloosahatchee River discharges and nitrogen inputs systematically intensify blooms.
- Anthropogenic influence extends upstream to Lake Okeechobee and the Kissimmee basin.
- Nutrient/hydrological management may mitigate bloom intensity and duration.

GRAPHICAL ABSTRACT

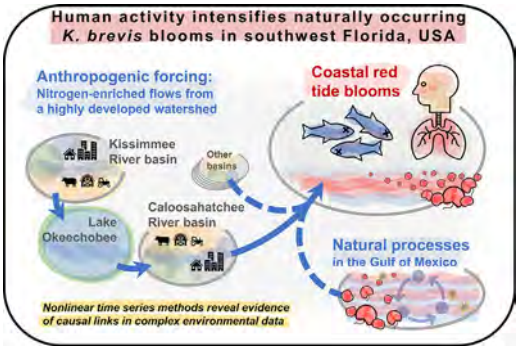

ARTICLE INFO

Article history:
Received 31 December 2021
Received in revised form 21 February 2022
Accepted 22 February 2022
Available online 25 February 2022

Editor: Fernando A.L. Pacheco

Keywords:
Harmful algal bloom (HAB)
Lake Okeechobee
Charlotte Harbor
Eutrophication
Chaos
Nonlinear dynamics

ABSTRACT

Karenia brevis blooms on Florida's Gulf Coast severely affect regional ecosystems, coastal economies, and public health, and formulating effective management and policy strategies to address these blooms requires an advanced understanding of the processes driving them. Recent research suggests that natural processes explain offshore bloom initiation and shoreward transport, while anthropogenic nutrient inputs may intensify blooms upon arrival along the coast. However, past correlation studies have failed to detect compelling evidence linking coastal blooms to watershed covariates indicative of anthropogenic inputs. We explain why correlation is neither necessary nor sufficient to demonstrate a causal relationship—i.e., a persistent pattern of interaction governed by deterministic rules—and pursue an empirical investigation leveraging the fact that systematic temporal patterns may reveal systematic cause-and-effect relationships. Using time series derived from in-situ sample data, we applied singular spectrum analysis—a non-parametric spectral decomposition method—to recover deterministic signals in the dynamics of *K. brevis* blooms and upstream water quality and discharge covariates in the Charlotte Harbor region between 2012 and 2021. Next, we applied causal analysis methods based on chaos theory—i.e., convergent cross-mapping and S-mapping—to detect and quantify persistent, state-dependent interaction regimes between coastal blooms and watershed covariates. We discovered that nitrogen-enriched Caloosahatchee River discharges have consistently intensified *K. brevis* blooms to varying degrees over time. River discharge was typically most influential at the earliest stages of blooms, while total nitrogen concentrations exerted the strongest influence during blooms' growth/maintenance stages. These results indicate that discharges and nitrogen inputs influence blooms through distinct yet synergistic causal mechanisms. Additionally, we traced this anthropogenic influence upstream to Lake Okeechobee (which discharges to the Caloosahatchee River)

* Corresponding author at: 365 Weil Hall, Gainesville, FL 32611, United States.
E-mail address: miles.medina@ufl.edu (M. Medina).

http://dx.doi.org/10.1016/j.scitotenv.2022.154149

and the Kissimmee River basin (which drains into Lake Okeechobee), suggesting that watershed-scale nutrient management and modifications to Lake Okeechobee discharge protocols will likely be necessary to mitigate coastal blooms.

1. Introduction

Harmful algal blooms (HABs) are complex phenomena whose mechanistic drivers vary by locale, by species, and by bloom event (Anderson et al., 2012; Anderson et al., 2021; Vargo, 2009). Describing the mechanisms that give rise to these blooms has been the subject of intense research effort aimed at supporting the development of effective prevention and mitigation strategies (Anderson et al., 2012; Anderson et al., 2021; Paerl et al., 2018). Along Florida's Gulf Coast (USA), blooms of *Karenia brevis*—a mixotrophic marine dinoflagellate—threaten public health, interrupt economic activity, and contribute to ongoing degradation of ecological communities (Anderson et al., 2021; Backer, 2009; Bechard, 2021; Court et al., 2021; Sonak et al., 2018). Recent research indicates that the development of these blooms is determined by both natural and anthropogenic processes and their interactions: Atmospheric, biological, and oceanographic processes explain offshore bloom initiation in the Gulf of Mexico and advection of blooms toward the coast (Steidinger, 2009; Walsh et al., 2006; Weisberg et al., 2019), while altered discharge and nutrient loading regimes associated with urban and agricultural development may intensify blooms upon their arrival along the coast (Anderson et al., 2008; Heil et al., 2014b; Medina et al., 2020).

The role of anthropogenic forcing in the coastal *K. brevis* bloom phenomenon is not well resolved—a knowledge gap, that if filled, would reveal opportunities to mitigate bloom intensity, duration, and impacts, along with other water quality problems linked to eutrophication, such as hypoxia (Milbrandt et al., 2021; Vargo, 2009) and macroalgae blooms (Milbrandt et al., 2019). This study empirically investigates the dynamics of coastal *K. brevis* blooms in southwest Florida and several watershed covariates along a major flow path to the coast, to identify persistent and systematic anthropogenic drivers of blooms as targets for management and policy intervention. We focus on *K. brevis* blooms between Charlotte Harbor and the Caloosahatchee River (Fig. 1), a region whose wildlife, public health, and economic activity have suffered adverse impacts (Court et al., 2021; Gravinese et al., 2020; Milbrandt et al., 2021; Sonak et al., 2018).

Past empirical investigations of 'the anthropogenic hypothesis'—that anthropogenic nutrient inputs intensify *K. brevis* blooms along Florida's Gulf Coast—support its mechanistic plausibility. Using paleo-indicators, Turner et al. (2006) estimated a threefold increase in nitrogen (N) loading to Charlotte Harbor between 1800 and 2000, associated with population growth and land use intensification. Heil et al. (2014b) found that terrestrial nutrient loads can substantially contribute to the nutrient requirements of small estuarine blooms ($<10^5$ cells/l), providing up to 17% of N and 69% of phosphorus (P) during dry years, and up to 100% of N and P during wet years.

Other empirical studies probing a direct link between anthropogenic nutrients and *K. brevis* blooms along the Gulf Coast have focused on correlation analysis and have yielded mixed evidence. For instance, Dixon and Steidinger (2002) found that coastal *K. brevis* presence was significantly correlated with discharges (with short time lags) from most rivers along Florida's central and southern Gulf Coast between 1953 and 1998. Notably, however, these authors found no such correlation with Caloosahatchee River discharges, speculating that nutrient loading, not discharge, was the relevant factor (Dixon and Steidinger, 2002). Later, Dixon et al. (2014) found no clear links between *K. brevis* blooms and terrestrial nutrient inputs across a large study area, from Tampa Bay to the Caloosahatchee estuary, between 2007 and 2010.

This mixed evidence enables persistent uncertainty about whether anthropogenic forcing of blooms is sufficiently resolved to justify management and policy intervention. To help resolve these inconsistencies, we point out that the anthropogenic hypothesis is fundamentally a causal hypothesis and that correlations are often not a reliable test of causal hypotheses about complex, open systems (Deyle et al., 2016; Sugihara et al., 2012). First, a significant correlation between coastal eutrophication and HABs would not necessarily evince a causal connection, since the correlation might simply reflect coincidental seasonal forcing. Inversely, a lack of correlation does not necessarily imply a lack of causation, since correlations detect only simple relationships—i.e., proportional or monotonic responses (see demonstration in Fig. 2). As such, variables in a complex system may consistently interact and yet show no correlation, or exhibit 'mirage correlations' that vary in magnitude and direction over time (Sugihara et al., 2012).

There is good reason to suspect that causality between coastal eutrophication and HABs cannot be reliably detected simply by assessing correlations (Anderson et al., 2012). Nutrient/discharge-HAB interactions are typically *state-dependent*, such that the magnitude of interaction varies over time as a function of multiple dynamic variables in the system (Isles and Pomati, 2021; McGowan et al., 2017; Medina et al., 2020). In Florida, coastal *K. brevis* blooms—which exist at the interface of dynamic oceanographic and watershed processes—depend on nutrient and salinity conditions influenced by tides and circulation, pelagic and benthic nutrient fluxes, freshwater inputs from the land, watershed-sourced nutrient fluxes, and coastal nutrient recycling (Dixon and Steidinger, 2002; Heil et al., 2014b; Steidinger, 2009; Vargo, 2009). Engineered management of flows (i.e., Lake Okeechobee discharges via the Caloosahatchee River) and growing urban development on the coast introduce additional complexity and, potentially, nonstationarities in the relationships among nutrients, discharges, and blooms.

To investigate the anthropogenic *K. brevis* hypothesis, we adopt a deterministic approach that avoids the limitations of statistical correlation. Central to this paradigm is the concept of *phase space* (Fig. 2C), a representation of system dynamics that facilitates investigation of causal hypotheses in a state-dependent context (Sugihara et al., 2012). As in the familiar scatterplot, the axes defining a phase space correspond to variables, and the coordinates of each point in the space are a unique combination of the states of these variables (Nolte, 2010). Thus, the phase space of a system represents all possible system states, and an important feature of the space is that neighboring points correspond to similar states. For a certain class of complex systems—*dissipative* systems—the evolution of the system in time traces a trajectory through phase space along a *manifold*, an object whose topology (shape) encodes the rules governing the variables' interactions (Kaplan and Glass, 1995). The deterministic rules of a dissipative system constrain the manifold to a compact, *low-dimensional* region of phase space, enabling analysis of the system with respect to only a small set of variables (Kaplan and Glass, 1995). In practice, however, we lack full information on system dynamics (i.e., data on every variable) and cannot observe the true manifold. Instead, we can draw inferences from low-dimensional *shadow manifolds*—phase space reconstructions built from time series of one or more variables—given that these reconstructions preserve information encoded in the true, unobserved manifold (Deyle and Sugihara, 2011; Takens, 1981).

Low-dimensional phase space representations enable causal inference because interacting variables detectably share information such that the history of any one variable in a system potentially encodes information about its drivers' dynamics (Sugihara et al., 2012). For the purposes of this study, therefore, we use the term 'causality' to refer to a systematic and persistent pattern of interaction governed by deterministic rules, in contrast with, for instance, responses to stochastic pulse disturbances. This form of investigation of causes and effects respects the dynamic, state-dependent nature of interactions in complex systems (encoded in the topology of the manifold), in contrast to correlation tests and other statistical procedures that reduce interactions to static processes (Fig. 2D) (Deyle et al., 2016; Sugihara et al., 2012).

Using phase space methods, Medina et al. (2020) recently detected a causal link between *K. brevis* blooms near Charlotte Harbor and N

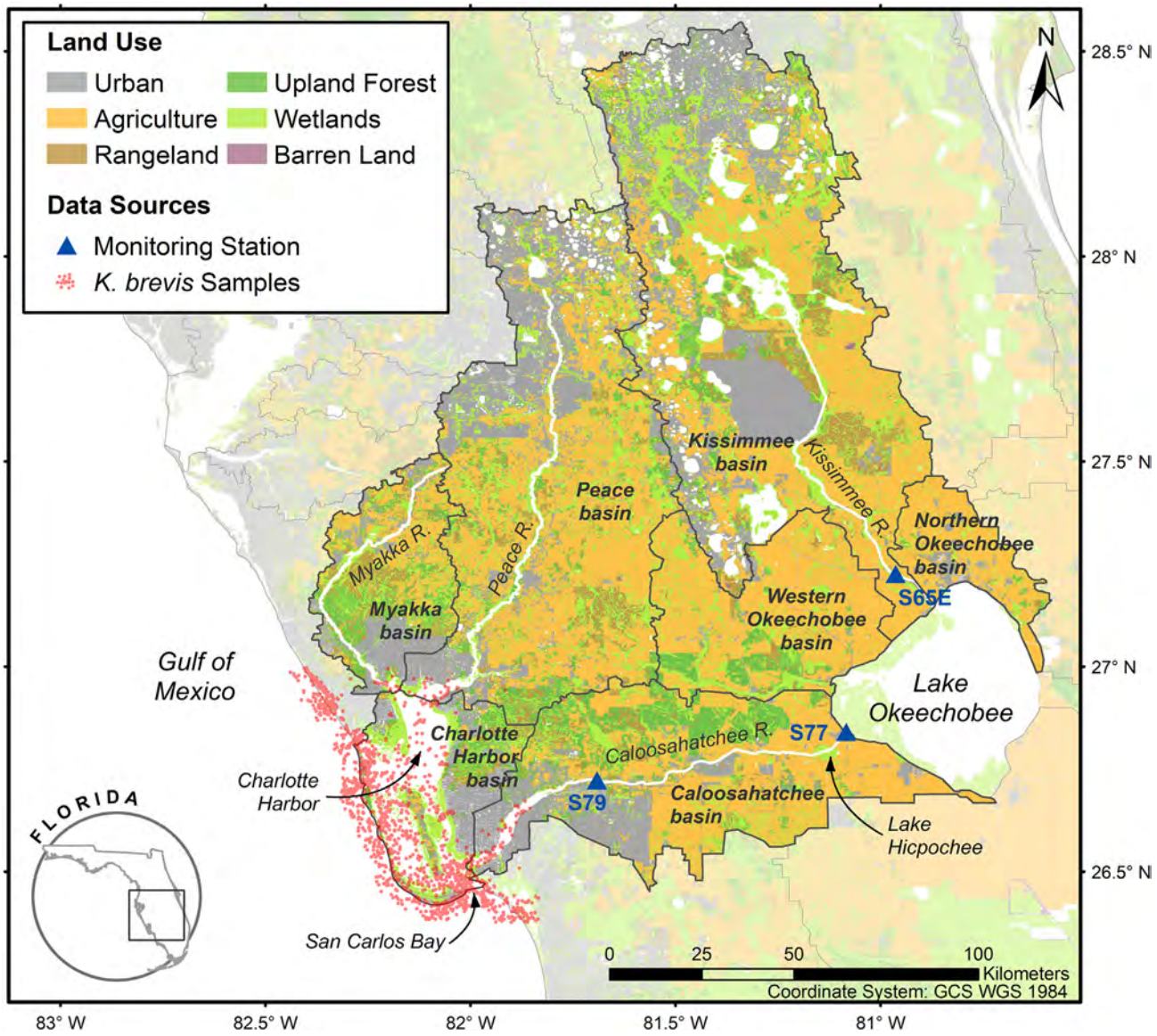

Fig. 1. Southwest Florida study area. The Charlotte Harbor estuary watershed comprises seven HUC-8 basins (HUC: Hydrologic Unit Code), outlined in black, and three main rivers. The Caloosahatchee River conveys discharges from Lake Okeechobee, which drains the predominantly agricultural Kissimmee, Northern Okeechobee, and Western Okeechobee basins. Red points indicate *K. brevis* sample locations (n = 18,160) near Charlotte Harbor and the Caloosahatchee estuary, within 1.61 km (1 mi) of the coastline and latitude bounds (26.375°, 27°), between January 2005 and February 2021. Discharge and water quality data were obtained from the following flow control structures (blue triangles): the Caloosahatchee River estuary (S79), Lake Okeechobee discharge to the Caloosahatchee River (S77), and Kissimmee River discharge to Lake Okeechobee (S65E). GIS shapefiles for land use and HUC-8 boundaries provided by Florida Department of Environmental Protection (2016) and Florida Department of Environmental Protection (2017).

concentrations in Caloosahatchee River discharges between 2012 and 2018. However, the study left several important questions unanswered. First, the study limited investigation to causal connections occurring within the same 14-day time step and did not account for delayed effects. Second, the study did not characterize the nature of the relationship between N inputs and *K. brevis* blooms. For instance, it is possible that N-enriched discharges strictly facilitate, or intensify, blooms (a positive relationship). Alternatively, the sign of the interaction may vary in time—at times facilitative due to N inputs and at other times inhibitive due to, for instance, the associated influx of low-salinity freshwater. Finally, the study did not resolve whether the influence of Caloosahatchee River N dynamics on *K. brevis* blooms could be traced upstream to Lake Okeechobee and the Kissimmee River basin, which would imply influence from a vast watershed beyond the lands and waterways immediately adjacent to the coast.

The current study sheds further light on the persistent causal influence of anthropogenic processes—in particular, nutrient-enriched discharges—on *K. brevis* blooms near Charlotte Harbor, by investigating the following hypotheses (Fig. 3A):

Hypothesis 1. Nutrient-enriched discharges from the Caloosahatchee River systematically facilitate (intensify) *K. brevis* blooms near Charlotte Harbor and the Caloosahatchee estuary.

Hypothesis 2. This facilitative influence reaches upstream to Lake Okeechobee and the Kissimmee River, which drains into Lake Okeechobee.

2. Methods

2.1. Overview

We tested the two hypotheses in sequence; the results from testing the first hypothesis informed the testing of the second (Fig. 3A). Our

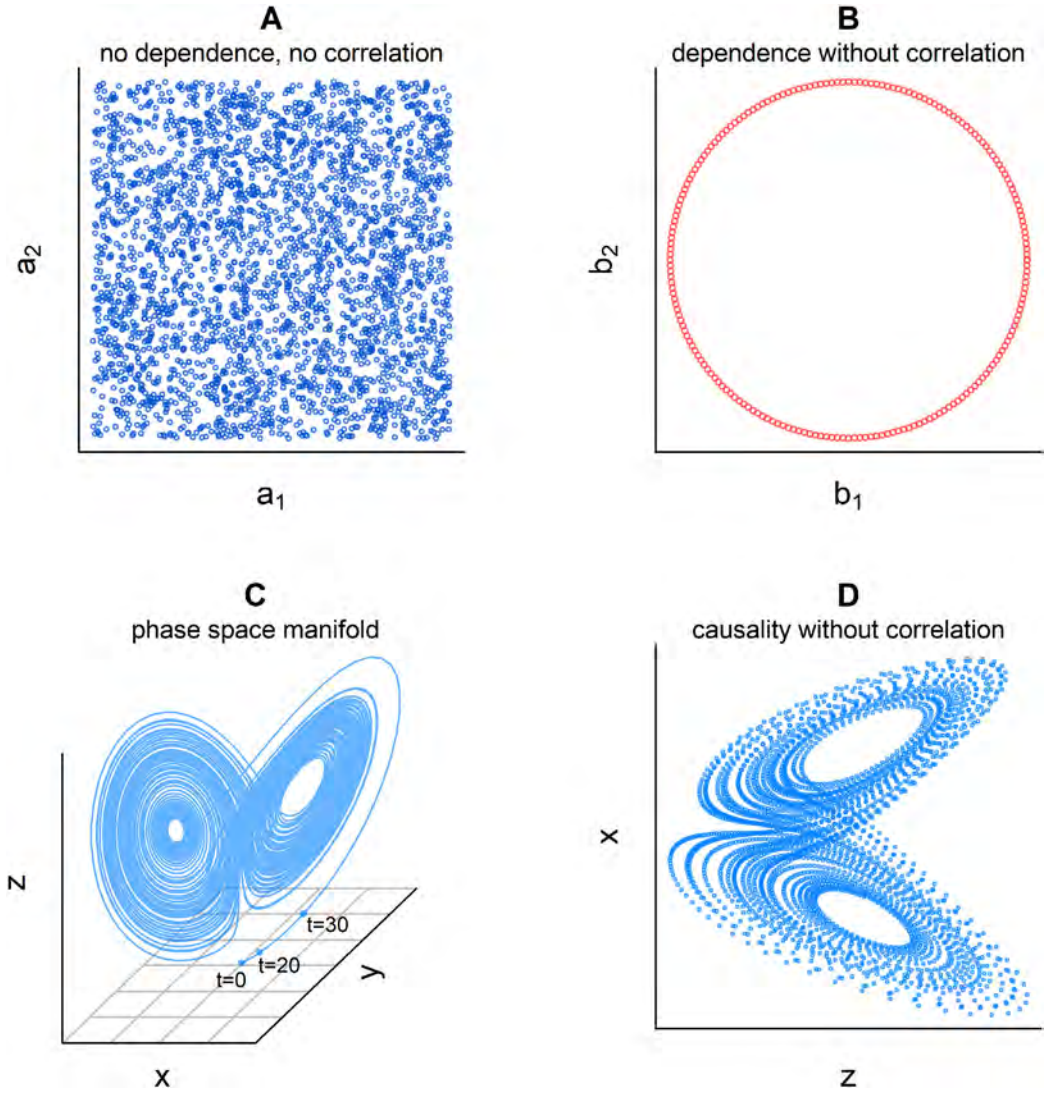

Fig. 2. Correlation and causality. In (A), a scatterplot of two sets of random values shows their lack of correlation. However, in (B), two variables with a clearly dependent relationship are also uncorrelated (the best-fit line has zero slope). In (C), we provide the phase space representation of a system of three variables (x, y, z) that causally interact according to deterministic rules; these are simulated data from the differential equation model of Lorenz (1969). Starting from time $t = 0$, the system state traces a trajectory through phase space as it evolves in time (a few points along the early trajectory are labeled). The system orbits along a manifold, or attraction basin, whose shape encodes the rules (equations) governing the dynamic state-dependent interactions among x, y, and z. In (D), a scatterplot of two Lorenz variables shows a lack of correlation despite the variables' underlying causal relationship. Further, if we consider subsets of the plotted data, correlations would be misleading: Different subsets may show positive correlation (data in the upper lobe), negative correlation (lower lobe), or no correlation.

investigation follows the workflow in Fig. 3B. First, we built time series from in-situ discharge data and water quality sample data: *K. brevis* concentrations, N and P concentrations, and specific conductance. From each time series, we attempted to recover a temporally structured *signal* and reconstruct a shadow manifold; diagnostic procedures test these manifolds for nonlinear stationarity and low-dimensional, deterministic structure. Next, the presence of systematic patterns of behavior (signals) suggests the potential for systematic cause-and-effect mechanisms. We tested for hypothesized causal interactivity between covariate pairs (e.g., total nitrogen and *K. brevis*) by measuring correspondence between the associated shadow manifolds. In each case, the results were scrutinized to ensure that coincidence (shared seasonality) was not mistaken for true causality. For Hypothesis 1, we also quantified the interaction regime among *K. brevis* and its detected causal drivers, by constructing a low-dimensional manifold from the associated signals and analyzing its structure. Below, Sections 2.3 through 2.5 provide details on each of the methodological procedures.

2.2. Study area

The *K. brevis* study area comprises coastal areas including Charlotte Harbor, Gasparilla Sound, Pine Island Sound, Matlacha Pass, the Caloosahatchee River Estuary, San Carlos Bay, and parts of Estero Bay and the Gulf of Mexico (hereafter referred to collectively as "Charlotte Harbor estuary"), as described more precisely in the subsequent subsection. The Charlotte Harbor estuary receives N- and P-enriched freshwater from a large, highly developed, and hydrologically altered watershed representing approximately one-sixth of Florida's total area (Florida Department of Environmental Protection, 2016; Florida Department of Environmental Protection, 2017). The watershed comprises seven HUC-8 basins as delineated by the U.S. Geological Survey (USGS), and three main rivers—the Myakka, Peace, and Caloosahatchee—flow into the Charlotte Harbor estuary (Fig. 1).

Our study focuses on the highly managed flow path from the Kissimmee River to Lake Okeechobee to the Caloosahatchee River to the Charlotte

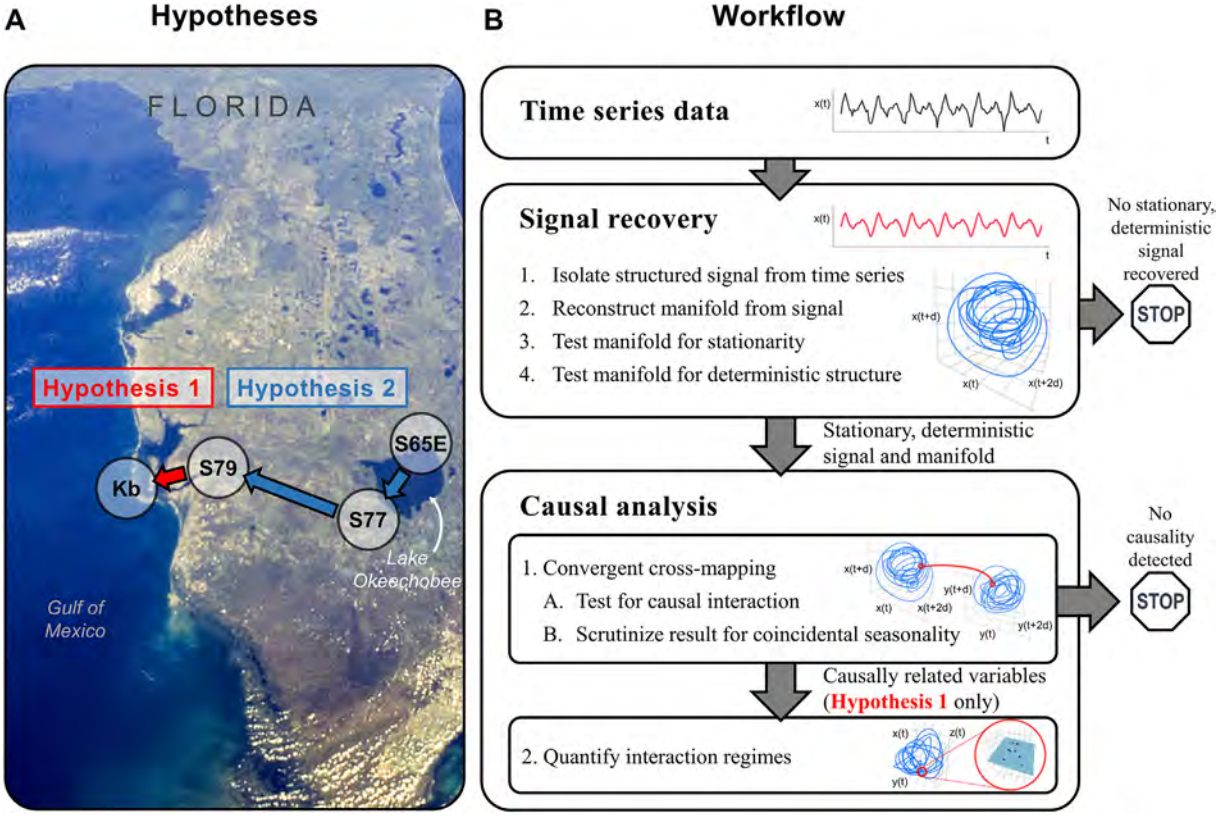

Fig. 3. Summary of hypotheses and empirical procedures. (A) Hypothesis 1 (red arrow) investigates discharge and water quality dynamics at S79 (Caloosahatchee River structure) as drivers of *K. brevis* blooms. Contingent on this investigation, Hypothesis 2 (blue arrows) investigates dynamics at S77 and S65E (Lake Okeechobee and Kissimmee River structures) as drivers of S79 conditions driving *K. brevis*. Photo credit: NASA. (B) A workflow for discovery of complex signals and causal connections. Investigation of interaction regimes (S-mapping) applies solely to Hypothesis 1.

Harbor estuary. The Kissimmee River drains a 7590 km^2 basin and is the main inflow to the eutrophic Lake Okeechobee. The Lake provides flood protection, drinking water, and agricultural irrigation water for South Florida, and the U.S. Army Corps of Engineers manages Lake discharges to the Gulf Coast via the Caloosahatchee River, to the Atlantic coast via the St. Lucie River, and south to the Everglades through a highly engineered system of canals and control structures. Historically, the Caloosahatchee River originated at Lake Hicpochee, but the 19th-century construction of a canal connecting Lakes Hicpochee and Okeechobee vastly expanded the watershed of the Caloosahatchee River beyond its own basin (3640 km^2) to include Lake Okeechobee and its watershed (Steinman et al., 2002).

Within the Kissimmee basin, land use is 44% agricultural/rangeland and 24% urban, and within the Caloosahatchee basin, land use is 46% agriculture/rangeland and 14% urban (Fig. 1; Florida Department of Environmental Protection, 2017). The agriculture/rangeland category encompasses a spatially heterogeneous mix of agricultural uses, including but not limited to grazing, improved pasture, dairy farms, row crops, and tree crops, that vary in terms of their characteristic impacts on water quality. A recent stable-isotope analysis identified agricultural nutrient runoff—in particular, runoff associated with summertime (wet season) application of ammonium (NH_4^+) fertilizers—as the primary source of nitrate (NO_3) within Lake Okeechobee (Ma et al., 2020). The urban land use category includes commercial, industrial, and low- to high-density residential developments, with spatially heterogeneous stormwater and sewage management, including onsite septic systems and centralized treatment infrastructure (Carey et al., 2012). Coastal urban developments within the study area contain high densities of septic systems along residential canals that are directly connected to the estuary (Buszka and Reeves, 2021).

Our choice to focus on the flow path through the Kissimmee basin, Lake Okeechobee, and the Caloosahatchee basin was primarily motivated by the recognition that the engineered management of Lake discharges affords unique opportunities to mitigate coastal *K. brevis* blooms, if these discharges are indeed identified as an important contributing factor. In addition, our analysis was constrained by data limitations, as the monitoring data from the Peace and Myakka Rivers were insufficient to construct time series of adequate length or resolution for analysis with phase space methods (i.e., fewer than five years of data and/or sampling frequency of less than one sample per 14 days). The basins that were excluded from our analysis—Myakka (1560 km^2), Peace (6070 km^2), Charlotte Harbor (1570 km^2), Western Okeechobee (2170 km^2), and Northern Okeechobee (790 km^2)—represent substantial land area and sources of flows and nutrients, and future analyses of watershed contributions to *K. brevis* blooms near Charlotte Harbor estuary should certainly consider these contributions.

The Florida wet season occurs during the summer (approximately June through September), and the area received mean annual rainfall of approximately 120 cm/yr between January 2012 and February 2021 (data from the Florida Automated Weather Network, http://fawn.ifas.ufl.edu/). Mean daily discharge at the Caloosahatchee River (station S79) was 5.80×10^6 m^3/d between January 2012 and February 2021.

2.3. Data

Karenia brevis concentration data (cells/l) were obtained from the NOAA Harmful Algal Blooms Observing System (HABSOS) database, version 5.5 (NOAA National Centers for Environmental Information, 2014); these data were provided to NOAA by the Florida Fish and Wildlife Conservation Commission. The dataset used for analysis includes n = 18,160 observations from the area bounded by latitudes 26.375° and 27.000° and within 1.61 km (1 mi) of the coastline between January 2005 and February 2021 (Fig. 1; see Video A.1). Some bias is to be expected in this dataset, since the *K. brevis* sampling regime includes both routine and event-based

sampling (not random). *Karenia brevis* blooms are typically seasonal, occurring in the fall following the summer rainy season. The maximum observed *K. brevis* concentration was 1.50×10^8 cells/l, and the mean was 1.65×10^5 cells/l. Most samples (90%) were collected at a depth of 0.5 m or less, and 99% of samples were collected at a depth of 5 m or less. *Karenia brevis* observations from the bounded area were aggregated to construct a time series with a two-week temporal resolution by computing the arithmetic mean of all available observations during each 14-day period. The two-week temporal resolution of the time series was determined by the availability of upstream water quality data, which were often collected at 14-day intervals, to minimize the need for imputation of missing values. The resulting time series was $\log_{10}$-transformed (zero values remained at zero). The log-transformed time series used for analysis represents the order of magnitude of *K. brevis* densities and emphasizes bloom events.

Water quality grab-sample data (total nitrogen, TN; total phosphorus, TP; nitrate + nitrite-N, NOx; orthophosphate-P, PO_4; and specific conductance, SpC) were obtained from the South Florida Water Management District (SFWMD) DBHYDRO database (https://www.sfwmd.gov/science-data/dbhydro). The sample locations (flow structures) include S79 at the lower Caloosahatchee River, S77 where Lake Okeechobee discharges into the Caloosahatchee River, and S65E where the Kissimmee River discharges Lake Okeechobee (Fig. 1). Some TN data were generated by summing concurrent NOx and TKN (total Kjeldahl nitrogen) observations. Water quality data flagged with fatal qualifier codes (Remark Codes *G*, *J*, *Q*, *V*, *Y*) or marked as field/equipment blanks or replicate samples (Sample Types *EB*, *FCEB*, *RS*) were removed from the dataset, according to the DBHYDRO User Guide (South Florida Water Management District [SFWMD], 2020). Non-detect values (Remark Code *U*) were replaced with the corresponding method detection limit. A time series for each water quality parameter at each station was constructed at a two-week resolution by computing the arithmetic mean of all available observations during each 14-day period to coincide with the two-week periods as determined by the *K. brevis* data (beginning on January 11, 2005). Several water quality time series include missing values (two-week periods with no available data) that were imputed by linear interpolation (see Table 1). To reduce the need for interpolation, we excluded all data prior to the earliest occurrence of two consecutive missing values. As such, water quality periods of record (PORs) vary. Daily discharge (Q) data from station S79 were likewise obtained from DBHYDRO and aggregated to construct a time series at a two-week resolution.

2.4. Signal recovery

Following Huffaker et al. (2016) and Medina et al. (2020), we applied signal processing and diagnostic procedures to isolate a signal representing systematic behavior in each time series, using all available data for each variable (PORs vary). Diagnostics test whether recovered signals exhibit stationarity and low-dimensional, deterministic structure, as required by the causal analysis that follows.

2.4.1. Signal processing

Environmental data typically contain noise representing observational error, high-dimensional processes, and exogenously forced extreme values (Regan et al., 2002; Uusitalo et al., 2015). We isolated temporally structured components of each time series (signal) from noise using singular spectrum analysis (SSA), a non-parametric spectral decomposition and reconstruction method, according to the procedures described below, following Ghil et al. (2002), Golyandina and Korobeynikov (2014), and Hassani (2007). Prior to SSA, each time series was centered by subtracting the mean of the series from each element, so that the signal strength reflects variance from the mean, rather than separation from zero. During SSA decomposition, a time series is represented as a sum of *eigentriple* components that are inspected to determine whether they should be grouped as part of the signal or the noise (see Appendix A for mathematical details). Signal components (trends and oscillations) exhibit the following characteristics: relatively large singular values, independence from other components (orthogonality), and, in the case of oscillations, peaks in the Fourier power spectrum. Next, during SSA reconstruction, the signal is obtained by summing the components corresponding to selected eigentriples (thus filtering out the noise components). The signal strength—the proportion of the time series' variance explained by the signal—is computed as the sum of the associated singular values, divided by the sum of all singular values in the decomposition. It is worth noting that the goal of SSA is not maximize signal strength, which can be arbitrarily increased by including more eigentriples as part of the signal. Instead, the goal is to recover any low-dimensional temporal structure present within the time series.

2.4.2. Phase space reconstruction

Each signal can potentially be used to reconstruct a shadow manifold (system dynamics) by embedding the signal in phase space. We used the time-delay embedding method of Takens (1981), which guarantees that the shadow manifold preserves the topology of the true (unobserved) manifold under certain conditions. Phase space coordinates for the shadow manifold are given by the normalized signal $x(t)$ (scaled on [0,1]) and a few $(m - 1)$ time-delayed copies $x(t + d)$, $x(t + 2d)$, …, where d is the embedding delay and m is the embedding dimension. Following Fraser and Swinney (1986), we set d as the first local minimum of the mutual information function, and following Kennel et al. (1992), we set m using a false nearest neighbors test. Shadow manifolds for low-dimensional, nonlinear-deterministic systems exhibit visually apparent organization or structure (aperiodic orbits).

2.4.3. Stationarity tests

Our analysis of causality assumes that the system's structure, or dynamical regime, has remained consistent throughout the study period—

Table 1
Signal processing and diagnostic results for *K. brevis* log-concentration and hypothesized drivers.

Variable	Period of record	Series length	Missing values[a]	Spectral peak[b] (wk)	Signal strength[c]	Embedding dimension	H_0 rejections[d] (surrogate tests)
K. brevis log(concentration)	2005-01-11–2021-02-16	421	0	53	66.2%	3	4/4
S79 discharge	2012-01-03–2021-05-25	246	0	55	66.6%	3	4/4
S79 specific conductance	2010-04-27–2021-05-25	290	0.3%	145	72.9%	3	3/4
S79 TN concentration	2011-06-21–2021-05-25	260	0.4%	52	48.9%	3	4/4
S79 NOx concentration	2009-03-17–2021-05-25	319	4.1%	53	61.6%	2	4/4
S79 TP concentration	2009-03-17–2021-05-25	319	4.1%	53	76.9%	3	2/4
S79 PO_4 concentration	2009-03-17–2021-05-25	319	4.1%	53	59.6%	3	4/4
S77 TN concentration	2010-03-30–2021-05-25	292	1.0%	53	45.0%	3	3/4
S77 NOx concentration	2005-01-11–2021-05-25	428	3.3%	107	21.2%	–	–
S65E TN concentration	2005-01-11–2021-05-25	428	7.0%	285	52.9%	3	3/4
S65E NOx concentration	2005-01-11–2021-05-25	428	8.4%	54	64.5%	3	3/4

[a] The number of missing values as a percentage of time series length.
[b] The inverse of the peak frequency computed by Fourier transformation.
[c] The percentage of variance explained by the signal.
[d] The number of rejections of the null hypothesis out of four surrogate data tests. Rejections provide evidence that signals capture low-dimensional deterministic structure.

i.e., stationarity. In the context of nonlinear systems, we tested each shadow manifold for *nonlinear stationarity* using space-time separation plots, in which a stationary manifold exhibits space-time curves that either saturate to or oscillate around a stable value (Provenzale et al., 1992). This sense of stationarity is different than weak stationarity (from linear time series analysis) evinced by constant statistical moments (mean and variance), since statistical moments may vary in a nonlinear system despite no changes in the manifold's structure (Kantz and Schreiber, 2004). Additional details are provided in Appendix A.

2.4.4. Surrogate data tests

The visual organization of a shadow manifold is insufficient to indicate low-dimensional determinism, because linear-stochastic processes (e.g., a limit cycle) may mimic this apparent structure (Theiler et al., 1992). Thus, we formulated a null hypothesis (i.e., the manifold's apparent structure is due to a linear-stochastic process) and tested it using surrogate data. For each shadow manifold, we generated two ensembles of surrogate manifolds—adjusted amplitude Fourier transform (AAFT) surrogates and pseudo-periodic surrogates (PPS)—and estimated null distributions of two statistics from each of these ensembles (Small and Tse, 2002; Theiler et al., 1992). These statistics include (1) nonlinear prediction skill, based on one-step-ahead, nearest-neighbors prediction; and (2) permutation entropy, which measures the information content of the signal, with relatively low entropy indicating determinism (Brandt and Pompe, 2002; Kaplan and Glass, 1995). Thus, four rank-order hypothesis tests were performed for each shadow manifold (two ensembles times two statistics). Each null distribution comprised statistics from 399 surrogates (number of surrogates $N = k/\alpha - 1 = 399$, with significance level $\alpha = 0.05$ and $k = 20$). Tests rejected the null hypothesis if the shadow manifold's prediction skill (permutation entropy) was among the k largest (smallest) values in the null distribution. Rejections are consistent with the claim that the signal reflects a low-dimensional, nonlinear-deterministic process and justifies low-dimensional causal inference as described below. Additional details are provided in Appendix A.

2.5. Causal analysis

The causal analysis includes manifold-based methods to identify causally related covariate pairs (Sugihara et al., 2012; Ye et al., 2015) and to quantify the interaction regime among selected covariates over time (Deyle et al., 2016; Sugihara et al., 2012). These analyses used data from January 2012 through February 2021.

2.5.1. Convergent cross-mapping

Two causally related variables share information such that the dynamics of the driver can be recovered from the dynamics of the response; this holds whether the driver and response interact directly or through one or more intermediate variables (Sugihara et al., 2012). Convergent cross-mapping (CCM) tests whether two variables are causally related by quantifying the structural correspondence between their shadow manifolds, as described below, following Sugihara et al. (2012). To test the hypothesis that x drives y, the CCM procedure y *xmap* x (read: 'y cross-map x') uses a nearest-neighbors algorithm to predict values of x (the *target*) using points on the shadow manifold (the *library*) reconstructed from the y signal. Note that the prediction direction (y *xmap* x) is the opposite of the causal direction (x drives y). The algorithm begins by predicting from a small, random subset of the full library and iteratively increases library size; causality is consistent with cross-map prediction skill that increases with library size and converges to a positive value in [0,1]. Cross-map skill is expressed as the Pearson correlation ρ between actual and predicted values of the target; reported skill values are the mean ρ from the largest 10% of libraries across 100 replicate tests.

Whereas CCM tests for causality within the same time step (two weeks), we used Extended CCM to test for delayed effects by using libraries to predict backward- and forward-lagged targets, following Ye et al. (2015) as described below. A delayed effect is apparent when cross-map skill peaks at a backward lag (cause precedes effect). Peak skill at a forward lag is consistent with an effect preceding the hypothesized cause, to indicate no causality in the hypothesized direction.

We further scrutinized CCM results to rule out the possibility that a detected causal relationship is spurious due to coincidental seasonality with no underlying causal mechanism. For each causally related pair, we tested the null hypothesis (coincidental seasonality without causality) at each non-positive time lag by bootstrapping 500 surrogate time series that maintain the signals' seasonality and comparing the original CCM result (cross-map skill) to the null distribution ($\alpha = 0.05$). Surrogates were constructed by approximating the signal's seasonal (52-week) cycle with a smoothing spline and shuffling the residuals (Park et al., 2021).

2.5.2. S-mapping

Due to state dependence, the magnitude and direction of a causal interaction may vary over time (Deyle et al., 2016). We applied S-mapping to quantify interaction regimes among selected causally related variables (identified by CCM) and to characterize the interactions as facilitative or inhibitive over time. Following Deyle et al. (2016) as described below, the S-mapping procedure embeds a low-dimensional manifold to compute the Jacobian matrix at each successive time step, using a locally weighted linear regression to estimate the local, approximately linear gradients (slopes) on the manifold. The elements of each Jacobian are first-order partial derivatives (gradients) evaluated at a particular point on the manifold, approximating the magnitude of interaction among variables at a given time step. For instance, if we are interested in the drivers of x, the first row of the Jacobian matrix for a manifold in x, y, z space provides the partial derivatives $\left\{\frac{\partial x(t+1)}{\partial x(t)}, \frac{\partial x(t+1)}{\partial y(t)}, \frac{\partial x(t+1)}{\partial z(t)}\right\}$ quantifying the effects of marginal increases in x, y, and z at time t on x at $t + 1$. A collection of successive partial derivatives at each t is a time series of interaction coefficients whose sign at a given time step may be positive or negative, indicating facilitative or inhibitive interaction, respectively.

The S-mapping procedure uses one tunable parameter, θ, that controls how strongly the regression is localized (Deyle et al., 2016). For $\theta = 0$, the regression is not localized, and the estimated gradients do not vary with location on the manifold, reflecting a state-*independent* interaction. Positive values of θ allow gradients to vary locally on the manifold (i.e., to vary over time), consistent with state dependence. As recommended by Deyle et al. (2016), we selected θ by optimizing on prediction error (mean absolute error, MAE).

2.6. Software

We performed SSA using CaterpillarSSA 3.40 (GistaT Group, 2010). All other procedures were performed in R 4.1.0 (R Core Team, 2021) with the following packages. Data processing and visualization: 'dplyr' (Wickham et al., 2021), 'plyr' (Wickham, 2011), 'tidyr' (Wickham, 2021), 'lubridate' (Grolemund and Wickham, 2011), 'rgdal' (Bivand et al., 2021), 'geosphere' (Hijmans, 2019), 'zoo' (Zeileis and Grothendieck, 2005), 'animation' (Xie, 2013). Phase space methods: 'tseriesChaos' (Di Narzo and Di Narzo, 2019), 'rEDM' (Park et al., 2021), 'fractal' (Constantine and Percival, 2014), 'fields' (Nychka et al., 2017), 'pdc' (Brandmaier, 2015), 'rgl' (Murdoch and Adler, 2021), 'quantreg' (Koenker, 2021), 'Matrix' (Bates and Maechler, 2021). Data and R scripts are publicly available (https://osf.io/ajf3h/).

3. Results

3.1. S79 and K. brevis

Signals recovered from the *K. brevis* and S79 time series indicated low-dimensional, nonlinear-deterministic dynamics—i.e., systematic patterns of behavior emerging from complex but structured underlying processes. The *K. brevis* log-concentration signal explained 66.2% of the variance in the time series and was dominated by a seasonal (i.e., annual) cycle (Fig. 4A; Table 1). The *K. brevis* shadow manifold (embedded in $m = 3$

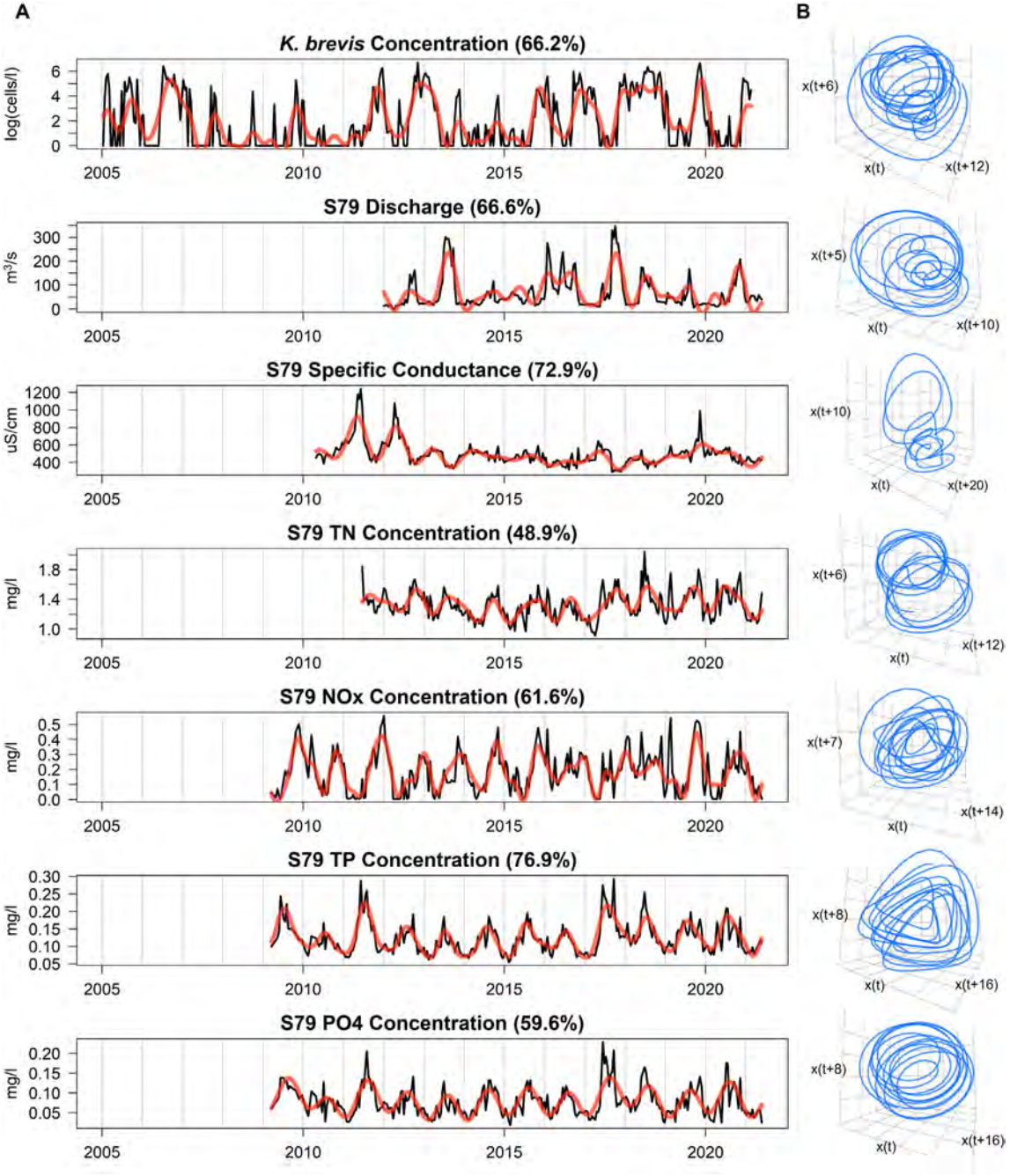

Fig. 4. Signals and shadow manifolds for *K. brevis* and S79 covariates. (A) Time series (black) and signals (red) for *K. brevis* concentrations and S79 covariates (Caloosahatchee River estuary), based on monitoring data from NOAA/HABSOS and SFWMD/DBHYDRO. The percentage of variance explained by each signal (signal strength) appears in parentheses. (B) 3-Dimensional projections of shadow manifolds reconstructed from the signals to the left.

dimensions) showed visually apparent structure (Fig. 4B), and diagnostic procedures indicated nonlinear stationarity and low-dimensional deterministic structure: Space-time curves oscillated around a stable value (Fig. A.1), and the null hypothesis of linear-stochastic dynamics was rejected by all four surrogate data tests (Tables 1, A.1). Likewise, all S79 covariates exhibited signals with a prominent seasonal component, with signal strengths ranging between 48.9% and 76.9%. Shadow manifolds for the S79 variables exhibited nonlinear stationarity (oscillating space-time curves) and low-dimensional deterministic structure (two or more rejections of the null hypothesis).

The recovery of systematic patterns of behavior in observed *K. brevis* dynamics implies that there is some structured causal mechanism (or mechanisms) that can potentially be inferred from the data. Extended CCM tests identified S79 discharge (Q), TN concentrations, and NOx concentrations as systematic drivers of *K. brevis* blooms (Fig. 5A). For each of these covariates, cross-map skill peaked at a negative lag, indicating delayed effects on *K. brevis* (Table 2). The results indicate that S79 TN and Q influence *K. brevis* with relatively short delays (on the order of one month), while the influence of S79 NOx occurs with a longer delay (several months). Seasonal surrogate tests of the S79 TN, NOx, and Q cross-mappings each rejected the null hypothesis of coincidental seasonal forcing ($P < 0.05$), consistent with a true causal relationship between each of these covariates and *K. brevis* (Table 2). Initially, S79 TP and PO_4 were identified as potential drivers of *K. brevis* (positive cross-map skill at negative lags), but surrogate data tests identified these results as false positives. The CCM results are summarized in a causal network diagram (Fig. 5B).

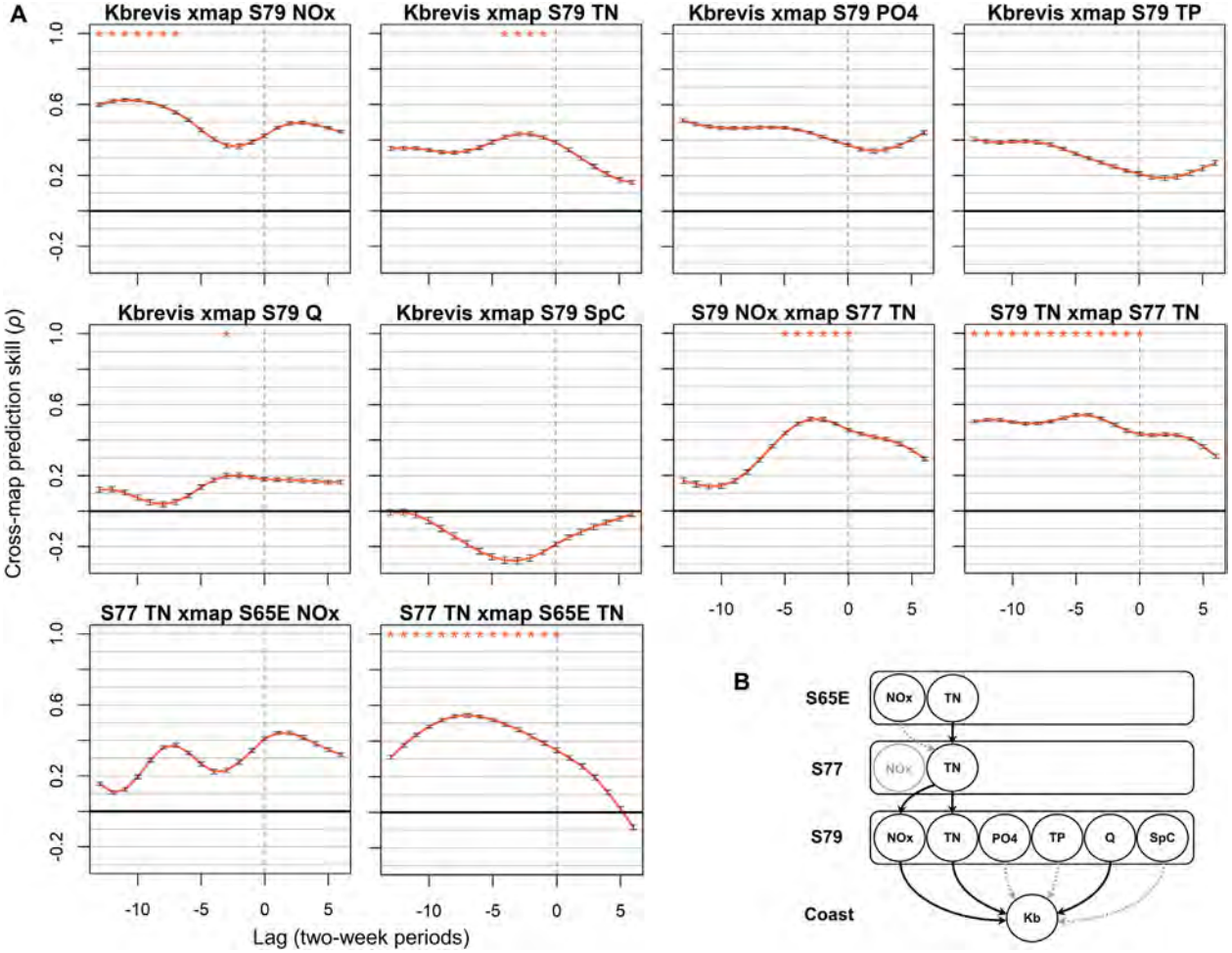

Fig. 5. CCM results. (A) Plots show cross-map prediction skill (ρ) against lags measured in two-week periods. Note that the cross-mapping "X xmap Y" represents the causal hypothesis "Y drives X." Red curves indicate mean ρ across lags, and error bars indicate standard deviations across 100 replicate cross-mappings. Red asterisks indicate lags at which the null hypothesis (coincidental seasonality) was rejected. (B) A causal diagram summarizes CCM results. Black arrows indicate causal relationships detected by CCM; gray arrows indicate CCM tests yielding negative results. Cross-mappings from coastal *K. brevis* (Kb) to S79 covariates identified S79 TN, NOx, and discharge (Q) as causal drivers; subsequently, we cross-mapped from NOx and TN upstream. CCM tests were not performed with S77 NOx (gray), because no signal was recovered from this time series.

Table 2
Summary of convergent cross-mapping (CCM) results (POR: January 2012 – February 2021).

CCM test	Peak cross-map skill[a]	Lag at peak skill[b]	Range of lags tested[b]	*P* value[c]
Hypothesis 1				
K. brevis xmap S79 NOx	0.63	−11	[−13,6]	0.002
K. brevis xmap S79 TN	0.44	−2	[−13,6]	0.032
K. brevis xmap S79 PO_4	0.51	−13	[−13,6]	0.481
K. brevis xmap S79 TP	0.41	−13	[−13,6]	0.529
K. brevis xmap S79 Q	0.20	−3	[−13,6]	0.036
K. brevis xmap S79 SpC	<0	–	[−13,6]	–
Hypothesis 2				
S79 NOx xmap S77 TN	0.52	−3	[−13,6]	0.002
S79 TN xmap S77 TN	0.54	−4	[−13,6]	0.002
S77 TN xmap S65E NOx	–	2	[−13,6]	–
S77 TN xmap S65E TN	0.54	−7	[−13,6]	0.002
K. brevis xmap S77 TN	–	5	[−26,13]	–
K. brevis xmap S65E TN	–	13	[−26,13]	–
K. brevis xmap S65E NOx	–	3	[−26,13]	–

[a] Peak skill among all lags tested.
[b] Lags are measured in two-week periods. Delayed effects are associated with negative lags. Peak skill at a positive lag indicates a false positive CCM result.
[c] Tests of the null hypothesis that cross-map skill reflects coincidental seasonality rather than true causality.

To quantify interactions among *K. brevis* drivers identified by CCM (S79 TN, S79 NOx, and S79 Q), we constructed 3- and 4-dimensional embeddings and selected the embedding that most skillfully predicted the *K. brevis* signal for S-mapping analysis. The optimal phase-space embedding ($\theta = 0.602$) included *K. brevis*, S79 TN, and S79 Q (Fig. 6A) and provided the basis for estimating interaction strength dynamics among these variables. Both interaction coefficient time series ($\frac{\partial Kb}{\partial TN}$ and $\frac{\partial Kb}{\partial Q}$) were variable, consistent with state dependence (Fig. 6B). The strictly positive sign of these interactions indicated that S79 TN and S79 Q consistently facilitated *K. brevis* blooms; this result was robust across all alternative 3- and 4-dimensional embeddings (Table A.2). In Fig. 6C and D, scatterplots of interaction coefficients (partial derivative values) against associated signals indicate that interaction magnitudes were relatively constant with respect to S79 TN and S79 Q but varied with respect to *K. brevis* log-concentrations. The facilitative influence of S79 Q was strongest when *K. brevis* concentrations were low and rising, early in the bloom cycle. In contrast, the facilitative influence of S79 TN was strongest later in the cycle, when *K. brevis* concentrations were high and blooms were at their peak (Fig. 6E).

3.2. Upstream causal connections

Based on our finding that TN and NOx concentrations at S79 intensify *K. brevis* blooms, we investigated N dynamics at upstream stations S77

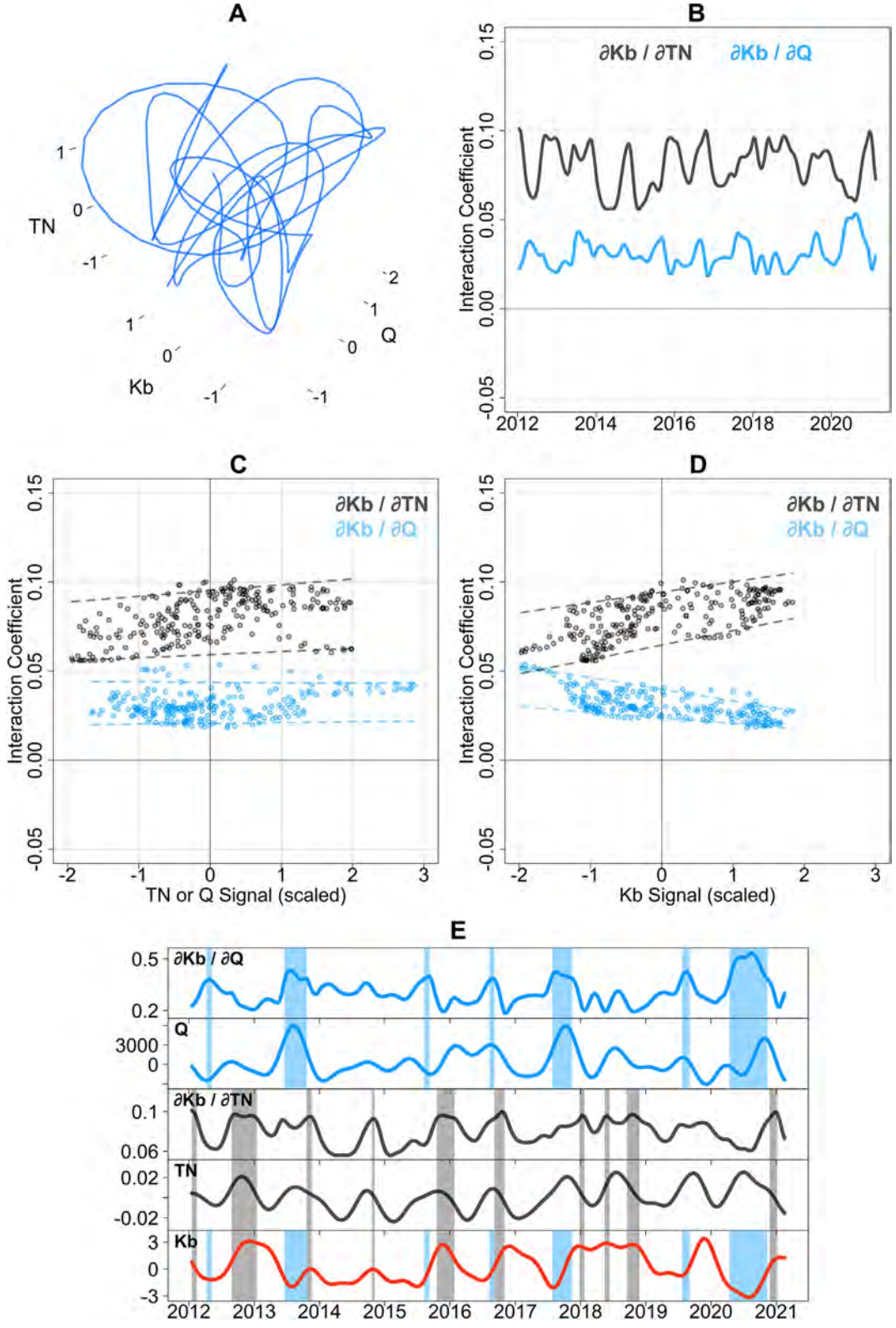

Fig. 6. S-map results. (A) The optimal phase-space embedding included S79 TN concentrations, TN; S79 discharge, Q; and *K. brevis* log-concentrations, Kb. Each axis is scaled to zero mean and unit variance. (B) Interaction time series (partial derivative vectors) quantify the change in Kb effected by changes in TN (black) and Q (blue) over time. (C, D) Scatterplots show relationships between these interaction strengths and their respective denominators (TN or Q, in panel C) and the numerator (Kb, in panel D). Horizontal axes are scaled to zero mean and unit variance, and dotted lines within plots indicate the 0.05 and 0.95 quantiles. (E) Stacked time series plots indicate the concurrence of the strongest interaction periods with associated signals. Based on an arbitrary threshold, the blue and gray regions highlight periods associated with the 80th percentile of $\frac{\partial Kb}{\partial Q}$ and $\frac{\partial Kb}{\partial TN}$ values, respectively.

and S65E (Lake Okeechobee and Kissimmee River control structures, respectively) and their causal connections to conditions at S79 (Hypothesis 2). The S77 TN, S65E TN, and S65E NOx time series exhibited signals (Fig. 7A) with strengths ranging between 45.0% and 64.5% (Tables 1, A.1). Shadow manifolds reconstructed from these signals exhibited visual regularity, nonlinear stationarity, and low-dimensional deterministic structure, as indicated by space-time plots and surrogate data tests (Fig. 7B, Table 1). In contrast, the S77 NOx time series did not exhibit a low-dimensional signal, and censoring the two large-magnitude observations did not substantially improve signal recovery.

Extended CCM tests indicated causal connections between N dynamics at S79 and at the S77 and S65E stations. In particular, S77 TN drove S79 TN and S79 NOx at zero lag and at several negative lags, with peak cross-map skill indicating a delay of one to two months (Fig. 5A). Likewise, S65E TN drove S77 TN concurrently and with delays, with peak cross-map skill indicating a delay of about three months. For each of these results, surrogate data tests rejected the null hypothesis of coincidental seasonality, consistent with true causality (Table 2). In contrast, we rejected S65E NOx as a driver of S77 TN, since cross-map skill was greatest at positive lags. The diagram in Fig. 5B summarizes these causal connections.

In addition, we applied Extended CCM to directly test for causal connections between *K. brevis* and the N covariates at S77 and S65E, over a larger range of lags, from −26 to 13 periods (−52 weeks to 26 weeks). The results showed no evidence of causality (Table 2; Fig. A.2). For *K. brevis xmap* S77 TN and for *K. brevis xmap* S65E TN, skill was near zero at non-positive lags. Skill was greater for *K. brevis* xmap S65E NOx, but the peak skill occurred at a positive lag.

4. Discussion

Population growth and land use intensification are associated with substantial N loading to Charlotte Harbor and Lake Okeechobee (Engstrom et al., 2006; Turner et al., 2006), and agricultural fertilizers and septic sewage are cited as major N sources within the Kissimmee and Caloosahatchee basins (Lapointe and Bedford, 2007; Ma et al., 2020). Within this context of persistent cultural eutrophication, we designed an empirical analysis to investigate a fundamental question: Does human activity systematically exacerbate *K. brevis* blooms near Charlotte Harbor? We hypothesized that (1) nutrient-enriched discharges from the Caloosahatchee River have systematically intensified *K. brevis* blooms near the Charlotte Harbor estuary, and (2) Lake Okeechobee and the Kissimmee basin contribute to this intensification. Our investigation expands on work by Medina et al. (2020), which linked S79 NOx concentrations to *K. brevis* bloom dynamics near Charlotte Harbor between 2012 and 2018. Our results support Hypothesis 1 as they affirm the link between *K. brevis* blooms and anthropogenic N inputs detected in this prior study over a longer time period (2012−2021) and indicate that discharges and N inputs from the Caloosahatchee River systematically *facilitate* blooms. We additionally traced the influence of N upstream to Lake Okeechobee and the Kissimmee basin (Hypothesis 2) and estimated time lags over which these causal connections manifest.

4.1. Bias in the K. brevis sample data

Sampling protocols for *K. brevis* include both routine sampling at fixed locations and event-based sampling, which introduces the potential for systematic bias to the extent that samples are collected when and where blooms are known to exist. One common concern is that event-based samples are likely upwardly biased relative to conditions across a wider area (Heil et al., 2014a). In addition, increased sampling effort during recent decades may give a false indication that cell counts have increased on annual or decadal timescales. Considering that our analytical approach was focused on patterns of behavior rather than changes in absolute magnitudes, however, a more important concern for our study was that preferential seasonal sampling (if present) may introduce a false seasonal signal. While some level of sampling bias is irreducible, we believe that aspects of the *K. brevis* sampling program, combined with our study design, reduced bias to an acceptable level.

Between January 2005 and February 2021, sampling effort was typically greatest during the months of October, November, and December, with a mean of 114 (±13 s.d.) samples per month, whereas the average

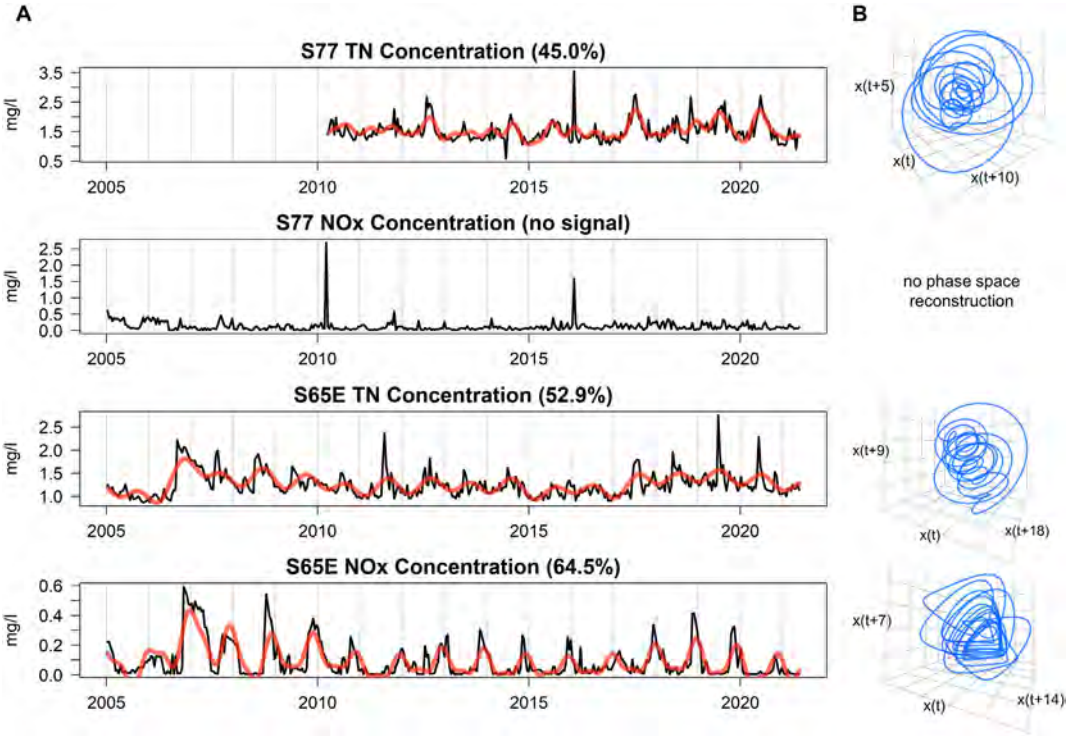

Fig. 7. Signals and shadow manifolds for S77 and S65E covariates. (A) Time series (black) and signals (red) for S77 and S65E covariates, based on monitoring data from SFWMD/DBHYDRO. The percentage of variance explained by each signal (signal strength) appears in parentheses. (B) 3-Dimensional projections of shadow manifolds reconstructed from the signals to the left.

for January through September was 87 (±8 s.d.) samples per month (Fig. A.3A). While this discrepancy should not be ignored, we applied SSA to the 14-day time series of sample counts and did not find evidence of strong, sustained seasonal bias (Fig. A.3B). Seasonal components (i.e., the annual cycle) of this time series explained only 9% of the series' variance, whereas longer-term trend components accounted for 44% of the variance, indicating that inter-annual differences in sampling effort were more important than intra-annual (seasonal) differences. In addition, the *K. brevis* sample data indicate good spatiotemporal coverage at the 14-day temporal resolution. The intervals between sampling events were typically short (Fig. A.3C): 84% of the intervals were less than one day (indicating two or more samples per day), and 10% were greater than one day and less than two days (samples on consecutive days). In terms of spatial coverage, in Video A.1, each frame visualizes *K. brevis* sample locations and magnitudes during a 14-day period. Each frame of this visualization indicates that sampling was distributed throughout the study area and shows several routine monitoring locations (points whose locations persist across frames), with few exceptions. Finally, spatiotemporal aggregation (averaging) and signal processing (SSA) of these sample data reduced the influence of high-magnitude event-based samples.

4.2. Interpretation of causal results

In this study, we sought to transcend the limitations inherent in applying correlation tests to analyze complex systems, with the goal of resolving ambiguities that have emerged from past empirical studies of the eutrophication-bloom relationship in southwest Florida (e.g., Dixon et al., 2014; Dixon and Steidinger, 2002). Our approach was motivated by the recognition that variables in a complex system may interact on a consistent basis and yet exhibit inconsistent correlations, which may or may not be meaningful (Sugihara et al., 2012). As such, we designed empirical analyses to test causal hypotheses in the context of state dependence and to guard against mistaking mere coincidence (shared seasonal forcing) for true causality. Our analysis focused on anthropogenic forcing along a major flow path to the Charlotte Harbor estuary, and the methods could likewise be applied to infer causal relationships among *K. brevis* blooms, their natural drivers, and anthropogenic forcings from other basins throughout the watershed (assuming the availability of sufficient data).

The CCM tests found the 'signature' of several S79 covariates in *K. brevis* bloom dynamics, indicating that Caloosahatchee River discharges and NOx and TN inputs systematically influenced *K. brevis* blooms near Charlotte Harbor. These results are particularly compelling considering the relatively large spatial domain of the *K. brevis* observations. Whereas it would not be unexpected to discover that S79 conditions are causally related to *K. brevis* dynamics in the immediate vicinity of the Caloosahatchee estuary, our results indicate that S79 conditions influence *K. brevis* bloom dynamics over a larger domain (Fig. 1).

When interpreting the time lags associated with each detected S79-bloom relationship (Fig. 5), one should consider that CCM was applied to spatiotemporally aggregated bloom data, and as such, the resulting lag estimates represent an aggregate over the full Charlotte Harbor estuary and study period. The real-world time lags likely vary at different locations within the study area at different times. Nonetheless, the detected time lags do suggest some interesting patterns. The relatively rapid effect of TN (2 to 8 weeks) on *K. brevis* concentrations, compared to the effect of NOx (14 weeks or more), indicate that *K. brevis* populations respond more quickly to estuarine inputs of organic N and/or NH_4^+ than to NOx inputs, and these results suggest distinct trophic and regeneration pathways for the various N constituents prior to assimilation by *K. brevis*. This interpretation is consistent with earlier studies indicating that dissolved organic N is typically relatively abundant in the Charlotte Harbor estuary (Bronk et al., 2014); *K. brevis* is nutritionally flexible and can take up organic N forms, such as urea, as well as inorganic N (Bronk et al., 2014); urea is associated with more rapid *K. brevis* cell division, as compared to inorganic forms (Sinclair et al., 2009); and the species has a greater affinity for NH_4^+ than NO_3^- and organic N, although organic N reduces to NH_4^+ (Bronk et al., 2014; Killberg-Thoreson et al., 2014).

The S-mapping results indicate that the net effect of N-enriched Caloosahatchee River discharges (S79) between 2012 and 2021 has been to intensify *K. brevis* blooms near Charlotte Harbor (Fig. 6B). While it is conceivable that discharges may at times simultaneously facilitate *and* inhibit blooms—e.g., large discharges might reduce estuarine salinity to less than optimal levels for *K. brevis* proliferation, or flush cells from the area—we found no evidence that any such inhibitive effect dominated the discharge-bloom interaction across the study area as a whole. The effects of both discharge and TN concentrations were consistently positive and sensitive to *K. brevis* levels. Discharge was most strongly influential when *K. brevis* concentrations were low and rising (Fig. 6E), indicating that Caloosahatchee River discharges play a role in the earliest stages of coastal blooms. This result points to several plausible mechanisms. One particularly intriguing possibility is that discharges facilitate advection and concentration of *K. brevis* cells into the Charlotte Harbor estuary by altering the area's hydrodynamics and enhancing the flood phase of tidal exchanges through San Carlos Bay and other inlets (Dye et al., 2020; Shi et al., in preparation). It is also possible that Caloosahatchee River discharges deliver iron or other nutrients that facilitate early population growth (Jones et al., 2011) and that large discharges mobilize benthic N (Seitzinger et al., 1991). Periods of relatively strong facilitation by discharge were typically followed by even stronger facilitation by TN concentrations, which exerted its greatest influence at the height of *K. brevis* bloom events (Fig. 6E), suggesting that anthropogenic TN helps to intensify, maintain, and thus prolong blooms. Collectively, these results suggest that it is not only the magnitude of discharges and TN loads that are important, but also the timing of these watershed inputs relative to a bloom's stage of development (and perhaps other factors).

Next, we investigated whether NOx and TN dynamics at S79 could be traced upstream to Lake Okeechobee (S77) and the Kissimmee basin (S65E). We adopted a 'daisy chain' strategy by proceeding upstream from S79 to S77 to S65E and testing whether N signals at each successive pair of stations showed evidence of a causal connection. Indeed, the results indicate that S65E TN signals drive S77 TN signals, which in turn drive S79 NOx and TN signals. The time lags associated with these causal connections ranged from zero up to the maximum value tested: 13 periods, or 26 weeks (Fig. 5A). The peak skill of the S79-S77 cross-mappings occurred at lags of 6 weeks (S79 NOx) and 8 weeks (S79 TN), consistent with estimated Caloosahatchee estuary residence times ranging between 4 and 60 days largely depending on S79 discharge (Wan et al., 2013). The peak skill of the S77 TN *xmap* S65E TN mapping occurred at 14 weeks, consistent with wind-driven circulation patterns and typical surface velocities in hydrodynamic simulations (Jin et al., 2000; Jin et al., 2002), despite nominal residence times on the order of several years (Janus et al., 1990). That we did not recover a signal in the S77 NOx time series or detect a causal link between S65E NOx and S77 TN is consistent with rapid denitrification and biological assimilation of inorganic N forms within Lake Okeechobee, where prior work has suggested that excessive P loading has shifted the Lake to a primarily N-limited regime (Havens, 1995; Ma et al., 2020). Collectively, the results of the causal analysis indicate that anthropogenic intensification of coastal *K. brevis* blooms involves discharges and N loads originating from a vast inland area (Lake Okeechobee and the Kissimmee basin) and imply that other areas that were not included in this analysis (e.g., the Peace and Myakka basins) may also substantially contribute to bloom intensification (Fig. 1).

We subsequently applied CCM to test more directly for causal connections between *K. brevis* and N covariates at S77 and S65E. The results were negative and point to the difficulty of detecting causality along a flow path that passes through multiple control structures within an intensively managed hydrological system. The negative results also point to the importance of other factors mediating watershed forcing of coastal *K. brevis* blooms, such as Caloosahatchee basin dynamics. Our analysis did not isolate the influence of the Caloosahatchee basin (S79 conditions integrate water quality conditions from this basin and the Lake), but past work indicates that this basin is an important source of N loads (Lapointe and Bedford, 2007; Rumbold and Doering, 2020).

In terms of nutrient limitation, for any biological response subject to a limiting factor (e.g., *K. brevis* blooms), one should expect the dynamics of that factor to exert a detectable influence on the response. As such, our results are suggestive of N limitation, consistent with observed coastal water column N:P ratios well below the Redfield ratio and an abundance of dissolved P attributed to inland phosphorite deposits and mining activity (Brand and Compton, 2007; Vargo, 2009; Walsh and Steidinger, 2001). Of course, these results do not imply that anthropogenic N inputs *alone* drive coastal *K. brevis* bloom intensification. These blooms represent a culmination of a complex set of dynamic factors and processes—including ocean circulation, salinity, availability of phosphate and other nutrients, and ecological interactions (Glibert et al., 2009; Paerl et al., 2018; Steidinger, 2009)—that may in turn influence the efficacy with which N inputs are converted into *K. brevis* biomass (state dependence). Further empirical investigation of the spatiotemporal dynamics of blooms' limiting (or co-limiting) factors may shed light on the mechanisms underlying coastal bloom intensification.

Finally, we emphasize that the anthropogenic and natural/oceanographic hypotheses are not mutually exclusive. Recent work has compellingly documented natural processes that explain offshore *K. brevis* bloom initiation in the Gulf of Mexico and the shoreward advection of cells (e.g., Weisberg et al., 2019; Weisberg et al., 2016). These authors have likewise acknowledged a role for anthropogenic forcing: "Eutrophication may help to maintain and intensify a *K. brevis* bloom once it manifests near shore" (Weisberg et al., 2016). Based on the evidence presented here and by Medina et al. (2020), we therefore call on researchers, managers, and policymakers to adopt a holistic view of the *K. brevis* problem—a view that considers both watershed and oceanographic processes and their interactions. A holistic approach is not only scientifically justified but also required if environmental policy and management are to succeed in mitigating bloom intensity and duration. Anthropogenic forcing can be managed and reduced with due effort, while natural forcing cannot.

4.3. Implications, study limitations, and future directions

Based on the persistent causal connection between N-enriched Caloosahatchee River discharges and nearby *K. brevis* blooms during the past decade, we encourage the research, management, and policy communities to continue efforts to develop and implement watershed-scale strategies to address the coastal *K. brevis* bloom problem. Our results serve as a valuable step forward by providing the scientific evidence needed to pursue opportunities to reduce coastal bloom intensity, duration, and, perhaps, frequency through strategic watershed nutrient management and Lake discharge operations with coincident benefits to reducing coastal eutrophication more generally. However, such strategies cannot be expected to eliminate blooms altogether, since offshore initiation and shoreward advection of blooms is well documented (e.g., Weisberg et al., 2019). Further investigation and modeling will be needed to quantify the extent to which policy and management interventions within the watershed can be expected to provide relief.

This study provides a robust and broadly applicable empirical framework for detecting systematic anthropogenic influence on coastal HABs in the context of complexity and state dependence. However, some key study limitations should be considered. We analyzed a coastal HAB phenomenon on a wide spatiotemporal scale by investigating basin-level watershed variables along a single flow path as drivers of blooms across a broad geographical area over a nearly ten-year period. Further, the study was designed to detect patterns of causal influence over time, rather than articulate the causal mechanisms underlying singular events. As such, this relatively high-level study was not designed to describe dynamics at fine spatial or temporal scales, provide a comprehensive mechanistic explanation of the bloom phenomenon, or account for all anthropogenic factors and processes that may affect bloom dynamics. In addition, this study did not engage with the overarching effects of global climate change, sea level rise, and associated salinity gradient changes.

To address these limitations and advance understanding of the role of anthropogenic processes in *K. brevis* blooms near Charlotte Harbor, further work will be required to

(1) identify agricultural and urban sub-basins throughout the watershed that most strongly facilitate coastal *K. brevis* blooms, as targets for nutrient source and transport control, using, for instance, additional data sources and spatiotemporal machine learning techniques (e.g. Wu et al., 2021);
(2) articulate at finer spatiotemporal resolutions the oceanographic and biogeochemical mechanisms of anthropogenic forcing, including discharge-induced changes to the estuary's hydrodynamics/circulation and nutrient transport, transformations, and assimilation by *K. brevis*;
(3) forecast the extent to which nutrient and hydrological management efforts throughout the watershed would mitigate bloom intensity and duration; and.
(4) develop cost-effective policy, management, and engineering solutions, such as modifications to the Lake Okeechobee Regulation Schedule, to minimize HABs. Cost-benefit estimates should account not only for the benefits of bloom mitigation but also the additional benefits that would be realized by overall improvements to coastal water quality, such as reducing eutrophication and hypoxia, reducing habitat loss, and enabling restoration of ecosystem functions and services.

5. Conclusion

We empirically linked *K. brevis* bloom intensification along the southwestern coast of Florida to anthropogenic forcing from an expansive and highly developed watershed. While the results of this study are relevant to land-based nutrient management and policy in Florida, they are not necessarily generalizable to other areas, since the HAB phenomenon is typically complex, with drivers and causal structures that may vary by locale and by species. Nonetheless, characterizing anthropogenic forcing and identifying controlling mechanisms in the context of state dependence are critical to understanding watershed influences on downstream water quality and to developing effective policies and management strategies. The methodological framework applied in this study embodies a deterministic perspective from which to view environmental dynamics, whose complexity may conceal systematic behavior and causal relationships of relevance to environmental modelers, managers, and policymakers. The deterministic perspective potentially enables analysis of dynamic causal interactivity among climatological, hydrological, biological, ecological, and social subsystems, provided that the interactions are meaningfully governed by a stationary, low-dimensional dynamical regime and that the available data are of sufficient frequency and duration to resolve the dominant cycles of interest.

Supplementary data to this article can be found online at https://doi.org/10.1016/j.scitotenv.2022.154149.

CRediT authorship contribution statement

MM: Conceptualization; Data curation; Formal analysis; Investigation; Methodology; Project administration; Software; Validation; Visualization; Writing - original draft; Writing - review & editing.

DK: Conceptualization; Investigation; Project administration; Resources; Supervision; Writing - review & editing.

ECM: Conceptualization; Investigation; Writing - review & editing.

DT: Conceptualization; Investigation; Writing - review & editing.

RH: Methodology; Software; Resources; Validation; Writing - review & editing.

CA: Conceptualization; Funding acquisition; Investigation; Methodology; Project administration; Resources; Supervision; Writing - review & editing.

Declaration of competing interest

The authors declare that they have no known competing financial interests or personal relationships that could have appeared to influence the work reported in this paper.

Acknowledgments

The authors thank Maitane Olabarrieta (University of Florida) for her assistance with the interpretation of results and the Florida Fish and Wildlife Conservation Commission for its ongoing *K. brevis* data collection efforts. The authors acknowledge the following funding sources: NSF CAREER (#1652628) to CA; National Academy of Sciences Gulf Coast Early Career Research Fellowship to CA; and a private donation to the University of Florida.

References

Anderson, D.M., Burkholder, J.M., Cochlan, W.P., Glibert, P.M., Gobler, C.J., Heil, C.A., Vargo, V.A., 2008. Harmful algal blooms and eutrophication: examining linkages from selected coastal regions of the United States. Harmful Algae 8 (1), 39–53. https://doi.org/10.1016/j.hal.2008.08.017.

Anderson, D.M., Cembella, A.D., Hallegraeff, G.M., 2012. Progress in understanding harmful algal blooms: paradigm shifts and new technologies for research, monitoring, and management. Annu. Rev. Mar. Sci. 4, 143–176. https://doi.org/10.1146/annurev-marine-120308-081121.

Anderson, D.M., Fensin, E., Gobler, C.J., Hoeglund, A.E., Hubbard, K.A., Kulis, D.M., Trainer, V.L., 2021. Marine harmful algal blooms (HABs) in the United States: history, current status, and future trends. Harmful Algae 120, 101975. https://doi.org/10.1016/j.hal.2021.101975.

Backer, L.C., 2009. Impacts of Florida red tides on coastal communities. Harmful Algae 8, 618–622. https://doi.org/10.1016/j.hal.2008.11.008.

Bates, D., Maechler, M., 2021. Matrix: Sparse and Dense Matrix Classes and Methods (Version 1.3-3). Retrieved from. https://CRAN.R-project.org/package=Matrix.

Bechard, A., 2021. Gone with the wind: declines in property values as harmful algal blooms are blown towards the shore. J. Real Estate Financ. Econ. 62, 242–257. https://doi.org/10.1007/s11146-020-09749-6.

Bivand, R., Keitt, T., Rowlingson, B., 2021. rgdal: Bindings for the "Geospatial" Data Abstraction Library (Version R Package Version 1.5-23). Retrieved from. https://CRAN.R-project.org/package=rgdal.

Brand, L.E., Compton, A., 2007. Long-term increase in karenia brevis abundance along the Southwest Florida coast. Harmful Algae 6 (2), 232–252. https://doi.org/10.1016/j.hal.2006.08.005.

Brandmaier, A., 2015. Pdc: an R package for complexity-based clustering of time series. J. Stat. Softw. 67 (5), 1–23. https://doi.org/10.18637/jss.v067.i05.

Brandt, C., Pompe, B., 2002. Permutation entropy: a natural complexity measure for time series. Phys. Rev. Lett. 88 (17), 174102.

Bronk, D.A., Killberg-Thoreson, L., Sipler, R.E., Mulholland, M.R., Roberts, Q.N., Bernhardt, P.W., Heil, C.A., 2014. Nitrogen uptake and regeneration (ammonium regeneration, nitrification and photoproduction) in waters of the West Florida shelf prone to blooms of karenia brevis. Harmful Algae 38, 50–62. https://doi.org/10.1016/j.hal.2014.04.007.

Buszka, T.T., Reeves, D.M., 2021. Pathways and timescales associated with nitrogen transport from septic systems in coastal aquifers intersected by canals. Hydrogeol. J. 29, 1953–1964. https://doi.org/10.1007/s10040-021-02362-8.

Carey, R.O., Hochmuth, G.J., Martinez, C.J., Boyer, T.H., Nair, V.D., Dukes, M.D., Sartain, J.B., 2012. Regulatory and resource management practices for urban watersheds: the Florida experience. HortTechnology 22 (4), 418–429. https://doi.org/10.21273/HORTTECH.22.4.418.

Constantine, W., Percival, D., 2014. Fractal: Fractal Time Series Modeling and Analysis. Retrieved from. https://cran.r-project.org/package=fractal.

Court, C., Ferreira, J., Ropicki, A., Qiao, X., Saha, B., 2021. Quantifying the socio-economic impacts of harmful algal blooms in Southwest Florida in 2018. Retrieved from.

Deyle, E.R., May, R.M., Munch, S.B., Sugihara, G., 2016. Tracking and forecasting ecosystem interactions in real time. Proc. R. Soc. B Biol. Sci. 283 (1822), 20152258. https://doi.org/10.1098/rspb.2015.2258.

Deyle, E.R., Sugihara, G., 2011. Generalized theorems for nonlinear state space reconstruction. PLoS ONE 6 (3), e18295. https://doi.org/10.1371/journal.pone.0018295.

Di Narzo, A., Di Narzo, F., 2019. tseriesChaos: Analysis of Nonlinear Time Series (Version R Package Version 0.1-13.1). Retrieved from. https://cran.r-project.org/package=tseriesChaos.

Dixon, L.K., Kirkpatrick, G.J., Hall, E.R., Nissanka, A., 2014. Nitrogen, phosphorus and silica on the West Florida shelf: patterns and relationships with Karenia spp. Occurrence. Harmful Algae 38, 8–19. https://doi.org/10.1016/j.hal.2014.07.001.

Dixon, L.K., Steidinger, K.A., 2002. Correlation of Karenia brevis in the eastern Gulf of Mexico with rainfall and riverine flow. In: Steidinger, K.A., Landsberg, J.H., Tomas, C.R., Vargo, G.A. (Eds.), Harmful Algae 2002: Proceedings of the Xth International Conference on Harmful Algae. Florida Fish and Wildlife Conservation Commission, Florida Institute of Oceanography, and Intergovernmental Oceanographic Commission of UNESCO, St. Petersburg, FL, pp. 29–31.

Dye, B., Jose, F., Allahdadi, M.N., 2020. Circulation dynamics and seasonal variability for the Charlotte Harbor estuary, Southwest Florida coast. J. Coast. Res. 36 (2), 276–288. https://doi.org/10.2112/JCOASTRES-D-19-00071.1.

Engstrom, D.R., Schottler, S.P., Leavitt, P.R., Havens, K.E., 2006. A reevaluation of the cultural eutrophication of Lake Okeechobee using multiproxy sediment records. Ecol. Appl. 16 (3), 1194–1206. https://doi.org/10.1890/1051-0761(2006)016[1194:arotce]2.0.co;2.

Florida Department of Environmental Protection, 2016]. Florida Hydrologic Unit Code (HUC) Basins (Areas). Retrieved from http://publicfiles.dep.state.fl.us/OTIS/GIS/data/HUC_BASINS_AREAS.zip. Updated February 2021. Accessed October 2021.

[dataset] Florida Department of Environmental Protection, 2017. Statewide land use land cover. Retrieved from: https://publicfiles.dep.state.fl.us/otis/gis/data/STATEWIDE_LANDUSE.zip. Updated May 2021. Accessed September 2021.

Fraser, A.M., Swinney, H.L., 1986. Independent coordinates for strange attractors from mutual information. Phys. Rev. A 33 (2), 1134–1140. https://doi.org/10.1103/PhysRevA.33.1134.

Ghil, M., Allen, M., Dettinger, M., Ide, K., Kondrashov, D., Mann, M., Yiou, P., 2002. Advanced spectral methods for climatic time series. Rev. Geophys. 40 (1), 1–41.

GistaT Group, 2010. CaterpillarSSA (Version Version 3.40) St. Petersburg, Russia.

Glibert, P.M., Burkholder, J.M., Kana, T., Alexander, J.A., 2009. Grazing by karenia brevis on synechococcus enhances its growth rate and may help to sustain blooms. Aquat. Microb. Ecol. 55 (1), 17–30. https://doi.org/10.3354/ame01279.

Golyandina, N., Korobeynikov, A., 2014. Basic singular spectrum analysis and forecasting with R. Comput. Stat. Data Anal. 71, 934–954.

Gravinese, P.M., Munley, M.K., Kahmann, G., Cole, C., Lovko, V., Blum, P., Pierce, R., 2020. The effects of prolonged exposure to hypoxia and Florida red tide (Karenia brevis) on the survival and activity of stone crabs. Harmful Algae 98, 101897. https://doi.org/10.1016/j.hal.2020.101897.

Grolemund, G., Wickham, H., 2011. Dates and times made easy with lubridate. J. Stat. Softw. 40 (3), 1–25. https://doi.org/10.18637/jss.v040.i03.

Hassani, H., 2007. Singular spectrum analysis: methodology and comparison. J. Data Sci. 5, 239–257.

Havens, K., 1995. Secondary nitrogen limitation in a subtropical lake impacted by non-point source agricultural pollution. Environ. Pollut. 89 (3), 241–246. https://doi.org/10.1016/0269-7491(94)00076-P.

Heil, C.A., Bronk, D.A., Dixon, L.K., Hitchcock, G.L., Kirkpatrick, G.J., Mulholland, M.R., Garrett, M., 2014. The Gulf of Mexico ECOHAB: Karenia program 2006-2012. Harmful Algae 38 (C), 3–7. https://doi.org/10.1016/j.hal.2014.07.015.

Heil, C.A., Dixon, L.K., Hall, E., Garrett, M., Lenes, J.M., O'Neil, J.M., Weisberg, R.W., 2014. Blooms of Karenia brevis (Davis) G. Hansen & Ø. Moestrup on the West Florida Shelf: Nutrient sources and potential management strategies based on a multi-year regional study. Harmful Algae 38, 127–140. https://doi.org/10.1016/j.hal.2014.07.016.

Hijmans, R.J., 2019. Geosphere: Spherical trigonometry (Version R Package Version 1.5-10). Retrieved from. https://CRAN.R-project.org/package=geosphere.

Huffaker, R., Canavari, M., Munoz-Carpena, R., Campo-Bescos, M., Southworth, J., 2016. Demonstrating correspondence between decision-support models and dynamics of real-world environmental systems. Environ. Model. Softw. 83, 74–87.

Isles, P.D.F., Pomati, F., 2021. An operational framework for defining and forecasting phytoplankton blooms. Front. Ecol. Environ. 19 (8), 443–450. https://doi.org/10.1002/fee.2376.

Janus, L.L., Soballe, D.M., Jones, B.J., 1990. Nutrient budget analyses and phosphorus loading goal for Lake Okeechobee, Florida. SIL Proceedings 24 (1), 538–546. https://doi.org/10.1080/03680770.1989.11898795.

Jin, K., Hamrick, J.H., Tisdale, T., 2000. Application of three-dimensional hydrological model for Lake Okeechobee. J. Hydraul. Eng. 126 (10), 758–771. https://doi.org/10.1061/(ASCE)0733-9429(2000)126:10(758).

Jin, K., Ji, Z., Hamrick, J.H., 2002. Modeling winter circulation in Lake Okeechobee, Florida. J. Waterw. Port Coast. Ocean Eng. 128 (3), 114–125. https://doi.org/10.1061/(ASCE)0733-950X(2002)128:3(114).

Jones, M.E., Beckler, J.S., Taillefort, M., 2011. The flux of soluble organic-iron(III) complexes from sediments represents a source of stable iron(III) to estuarine waters and to the continental shelf. Limnol. Oceanogr. 56 (5), 1811–1823. https://doi.org/10.4319/lo.2011.56.5.1811.

Kantz, H., Schreiber, T., 2004. Nonlinear Time Series Anaysis. 2nd ed. Cambridge University Press, Cambridge.

Kaplan, D., Glass, L., 1995. Understanding Nonlinear Dynamics. Springer, New York.

Kennel, M.B., Brown, R., Abarbanel, H.D.I., 1992. Determining embedding dimension for phase-space reconstruction using a geometrical construction. Phys. Rev. A 45 (6), 3403–3411. https://doi.org/10.1103/PhysRevA.45.3403.

Killberg-Thoreson, L., Mulholland, M.R., Heil, C.A., Sanderson, M.P., O'Neil, J.M., Bronk, D.A., 2014. Nitrogen uptake kinetics in field populations and cultured strains of Karenia brevis. Harmful Algae 38, 73–85. https://doi.org/10.1016/j.hal.2014.04.008.

Koenker, R., 2021. quantreg: Quantile regression (Version 5.86). Retrieved from. https://CRAN.R-project.org/package=quantreg.

Lapointe, B.E., Bedford, B.J., 2007. Drift rhodophyte blooms emerge in Lee County, Florida, USA: evidence of escalating coastal eutrophication. Harmful Algae 6 (3), 421–437. https://doi.org/10.1016/j.hal.2006.12.005.

Lorenz, E., 1969. The predictability of a flow which possesses many scales of motion. Tellus 21, 289–307.

Ma, P., Zhang, L., Mitsch, W.J., 2020. Investigating sources and transformations of nitrogen using dual stable isotopes for Lake Okeechobee restoration in Florida. Ecol. Eng. 155, 105947. https://doi.org/10.1016/j.ecoleng.2020.105947.

McGowan, J.A., Deyle, E.R., Ye, H., Carter, M.L., Perretti, C.T., Seger, K.D., Sugihara, G., 2017. Predicting coastal algal blooms in southern California. Ecology 98 (5), 1419–1433. https://doi.org/10.1002/ecy.1804.

Medina, M., Huffaker, R., Jawitz, J.W., Muñoz-Carpena, R., 2020. Seasonal dynamics of terrestrially sourced nitrogen influence Karenia brevis blooms of Florida's southern Gulf Coast. Harmful Algae 98, 101900. https://doi.org/10.1016/j.hal.2020.101900.

Milbrandt, E.C., Martignette, A.J., Thompson, M.A., Bartleson, R.D., Phlips, E.J., Badylak, S., Nelson, N.G., 2021. Geospatial distribution of hypoxia associated with a Karenia brevis bloom. Estuar. Coast. Shelf Sci. 259, 107446. https://doi.org/10.1016/j.ecss.2021.107446.

Milbrandt, E.C., Reidenbach, L., Parsons, M., 2019. Determining the sources of macroalgae during beach stranding events from species composition, stable isotope analysis, and laboratory experiments. Estuar. Coasts 42 (3), 719–730. https://doi.org/10.1007/s12237-018-00489-8.

Murdoch, D., Adler, D., 2021. rgl: 3D Visualization Using OpenGL (Version 0.107.14). Retrieved from. https://CRAN.R-project.org/package=rgl.
NOAA National Centers for Environmental Information, 2014]. Physical and Biological Data Collected Along the Texas, Mississippi, Alabama, and Florida Gulf coasts in the Gulf of Mexico as Part of the Harmful Algal BloomS Observing System From 1953-08-19 to 2021-03-09 (NCEI Accession 0120767.5.5). Retrieved from https://www.ncei.noaa.gov/archive/accession/0120767 Updated April 2021. Accessed April 2021.
Nolte, D.D., 2010. The tangled tale of phase space. Phys. Today 63 (4), 33–38. https://doi.org/10.1063/1.3397041.
Nychka, D., Furrer, R., Paige, J., S., S., 2017. Fields: Tools for Spatial Data. (Version 12.3). University Corporation for Atmospheric Research, Boulder, CO, USA. Retrieved from www.image.ucar.edu/fields.
Paerl, H.W., Otten, T.G., Kudela, R.M., 2018. Mitigating the expansion of harmful algal blooms across the freshwater-to-marine continuum. Environ. Sci. Technol. 52, 5519–5529. https://doi.org/10.1021/acs.est.7b05950.
Park, J., Smith, C., Sugihara, G., Deyle, D., 2021. rEDM: Applications of Empirical Dynamic Modeling From Time Series (Version 1.9.1). Retrieved from. https://CRAN.R-project.org/package=rEDM.
Provenzale, A., Smith, L., Vio, R., Murante, G., 1992. Distinguishing between low-dimensional dynamics and randomness in measured time series. Physica D 58 (1–4), 31–49. https://doi.org/10.1016/0167-2789(92)90100-2.
R Core Team, 2021. R: A Language and Environment for Statistical Computing (Version 4.1.0). R Foundation for Statistical Computing, Vienna, Austria. https://www.R-project.org/.
Regan, H.M., Colyvan, M., Burgman, M.A., 2002. A taxonomy and treatment of uncertainty for ecology and conservation biology. Ecol. Appl. 12 (2), 618–628. https://doi.org/10.1890/1051-0761(2002)012[0618:ATATOU]2.0.CO;2.
Rumbold, D.G., Doering, P.H., 2020. Water quality and source of freshwater discharge to the Caloosahatchee Estuary, Florida: 2009–2018. Florida Scientist 83 (1), 1–20.
Seitzinger, S.P., Gardner, W.S., Spratt, A.K., 1991. The effect of salinity on ammonium sorption in aquatic sediments: implications for benthic nutrient recycling. Estuaries 14 (2), 167–174. https://doi.org/10.2307/1351690.
Shi, L., Ortals, C., Olabarrieta, M., Valle-Levinson, A., n.d. River discharge effects on tidal propagation, subtidal flows, and velocity asymmetry in a mixed diurnal-semidiurnal micro-tidal river estuary. In preparation.
Sinclair, G., Kamykowski, D., Glibert, P.M., 2009. Growth, uptake, and assimilation of ammonium, nitrate, and urea, by three strains of Karenia brevis grown under low light. Harmful Algae 8 (5), 770–780. https://doi.org/10.1016/j.hal.2009.02.006.
Small, M., Tse, C., 2002. Applying the method of surrogate data to cyclic time series. Physica D 164, 187–201.
Sonak, S., Patil, K., Devi, P., D'Souza, L., 2018. Causes, human health impacts and control of harmful algal blooms: a comprehensive review. Environ. Pollut. Protect. 3 (1), 40–55. https://doi.org/10.22606/epp.2018.31004.
South Florida Water Management District [SFWMD], 2020. DBHYDRO Browser User's Guide. West Palm Beach, FL.
Steidinger, K.A., 2009. Historical perspective on Karenia brevis red tide research in the Gulf of Mexico. Harmful Algae 8 (4), 549–561. https://doi.org/10.1016/j.hal.2008.11.009.
Steinman, A.D., Havens, K.E., Carrick, H.J., Vanzee, R., 2002. The past, present, and future hydrology and ecology of Lake Okeechobee and its watersheds. In: Porter, J.W., Porter, K.G. (Eds.), The Everglades, Florida Bay, and Coral Reefs of the Florida Keys: An Ecosystem Sourcebook. CRC Press, Boca Raton.
Sugihara, G., May, R., Hao, Y., Chih-hao, H., Deyle, E., Fogarty, M., Munch, S., 2012. Detecting causality in complex ecosystems. Science 338, 496–500.
Takens, F., 1981. Detecting strange attractors in turbulence. In: Rand, D.Y.L. (Ed.), Dynamical Systems and Turbulence. Springer, New York, pp. 366–381.
Theiler, J., Eubank, S., Longtin, A., Galdrikian, B., Farmer, J., 1992. Testing for nonlinearity in time series: The method of surrogate data. Physica D 58, 77–94.
Turner, R.E., Rabalais, N.N., Fry, B., Atilla, N., Milan, C.S., Lee, J.M., Tomasko, D.A., 2006. Paleo-indicators and water quality change in the Charlotte Harbor estuary (Florida). Limnol. Oceanogr. 51 (1), 518–533. https://doi.org/10.4319/lo.2006.51.1_part_2.0518.
Uusitalo, L., Lehikoinen, A., Helle, I., Myrberg, K., 2015. An overview of methods to evaluate uncertainty of deterministic models in decision support. Environ. Model. Softw. 63, 24–31. https://doi.org/10.1016/j.envsoft.2014.09.017.
Vargo, G.A., 2009. A brief summary of the physiology and ecology of Karenia brevis Davis (G. Hansen and Moestrup comb. nov.) red tides on the West Florida Shelf and of hypotheses posed for their initiation, growth, maintenance, and termination. Harmful Algae 8, 573–584. https://doi.org/10.1016/j.hal.2008.11.002.
Walsh, J.J., Jolliff, J.K., Darrow, B.P., Lenes, J.M., Milroy, S.P., Remsen, A., Bontempi, P.S., 2006. Red tides in the Gulf of Mexico: Where, when, and why? J. Geophys. Res. 111 (C11), C11003. https://doi.org/10.1029/2004JC002813.
Walsh, J.J., Steidinger, K.A., 2001. Saharan dust and Florida red tides: the cyanophyte connection. J. Geophys. Res. 106 (C6), 11597–11612. https://doi.org/10.1029/1999JC000123.
Wan, Y., Qiu, C., Doering, P., Ashton, M., Sun, D., Coley, T., 2013. Modeling residence time with a three-dimensional hydrodynamic model: linkage with chlorophyll a in a subtropical estuary. Ecol. Model. 268, 93–102. https://doi.org/10.1016/j.ecolmodel.2013.08.008.
Weisberg, R., Liu, Y., Lembke, C., Hu, C., Hubbard, K., Garrett, M., 2019. The coastal ocean circulation influence on the 2018 West Florida Shelf K. brevis red tide bloom. J. Geophys. Res. Oceans 124, 2501–2512. https://doi.org/10.1029/2018JC014887.
Weisberg, R.H., Zheng, L., Liu, Y., Corcoran, A.A., Lembke, C., Hu, C., Walsh, J.J., 2016. Karenia brevis blooms on the West Florida Shelf: A comparative study of the robust 2012 bloom and the nearly null 2013 event. Cont. Shelf Res. 120, 106–121. https://doi.org/10.1016/j.csr.2016.03.011.
Wickham, H., 2011. The split-apply-combine strategy for data analysis. J. Stat. Softw. 40 (1), 1–29. https://doi.org/10.18637/jss.v040.i01.
Wickham, H., 2021. tidyr: Tidy Messy Data (Version 1.1.3). Retrieved from. https://CRAN.R-project.org/package=tidyr.
Wickham, H., François, R., Henry, L., Müller, K., 2021. dplyr: A Grammar of Data Manipulation (Version 1.0.6). Retrieved from. https://CRAN.R-project.org/package=dplyr.
Wu, J., Song, C., Dubinsky, E.A., Stewart, J.R., 2021. Tracking major sources of water contamination using machine learning. Front. Microbiol. 11, 616692. https://doi.org/10.3389/fmicb.2020.616692.
Xie, Y., 2013. animation: An R package for creating animations and demonstrating statistical methods. J. Stat. Softw. 53 (1), 1–27. https://doi.org/10.18637/jss.v053.i01.
Ye, H., Deyle, E., Gilarranz, L., Sugihara, G., 2015. Distinguishing time-delayed causal interactions using convergent cross mapping. Sci. Rep. 5 (14750), 1–9. https://doi.org/10.1038/srep14750.
Zeileis, A., Grothendieck, G., 2005. zoo: S3 infrastructure for regular and irregular time series. J. Stat. Softw. 14 (6), 1–27. https://doi.org/10.18637/jss.v014.i06.